

High efficient catalytic degradation of tetracycline and ibuprofen using visible light driven novel Cu/Bi₂Ti₂O₇/rGO nanocomposite: Kinetics, intermediates and mechanism

Shanavas, S., Priyadharsan, A., Gkanas, E., Acevedo, R. & Anbarasan, P. M.

Author post-print (accepted) deposited by Coventry University's Repository

Original citation & hyperlink: Shanavas, S, Priyadharsan, A, Gkanas, E, Acevedo, R & Anbarasan, PM 2019, 'High efficient catalytic degradation of tetracycline and ibuprofen using visible light driven novel Cu/Bi₂Ti₂O₇/rGO nanocomposite: Kinetics, intermediates and mechanism' *Journal of Industrial and Engineering Chemistry*, vol. 72, pp. 512-528.

<https://dx.doi.org/10.1016/j.jiec.2019.01.008>

DOI 10.1016/j.jiec.2019.01.008

ISSN 1226-086X

Publisher: Elsevier

NOTICE: this is the author's version of a work that was accepted for publication in *Journal of Industrial and Engineering Chemistry*. Changes resulting from the publishing process, such as peer review, editing, corrections, structural formatting, and other quality control mechanisms may not be reflected in this document. Changes may have been made to this work since it was submitted for publication. A definitive version was subsequently published in *Journal of Industrial and Engineering Chemistry*, [72], (2019) DOI: 10.1016/j.jiec.2019.01.008

© 2017, Elsevier. Licensed under the Creative Commons Attribution-NonCommercial-NoDerivatives 4.0 International

<http://creativecommons.org/licenses/by-nc-nd/4.0/>

Copyright © and Moral Rights are retained by the author(s) and/ or other copyright owners. A copy can be downloaded for personal non-commercial research or study, without prior permission or charge. This item cannot be reproduced or quoted extensively from without first obtaining permission in writing from the copyright holder(s). The content must not be changed in any way or sold commercially in any format or medium without the formal permission of the copyright holders.

This document is the author's post-print version, incorporating any revisions agreed during the peer-review process. Some differences between the published version and this version

may remain and you are advised to consult the published version if you wish to cite from it.

High efficient catalytic degradation of tetracycline and ibuprofen using visible light driven novel Cu/Bi₂Ti₂O₇/rGO nanocomposite: Kinetics, intermediates and mechanism

Shanavas S^a, A. Priyadharsan^a, E. I. Gkanas^b, R. Acevedo^c, P. M. Anbarasan^a

^a *Nano and Hybrid Materials Laboratory, Department of Physics, Periyar University, Salem-636 011, India.*

^b *Hydrogen for Mobility Lab, Institute for Future Transport and Cities, Coventry University, Priory Street, Coventry, CV1 5FB, UK*

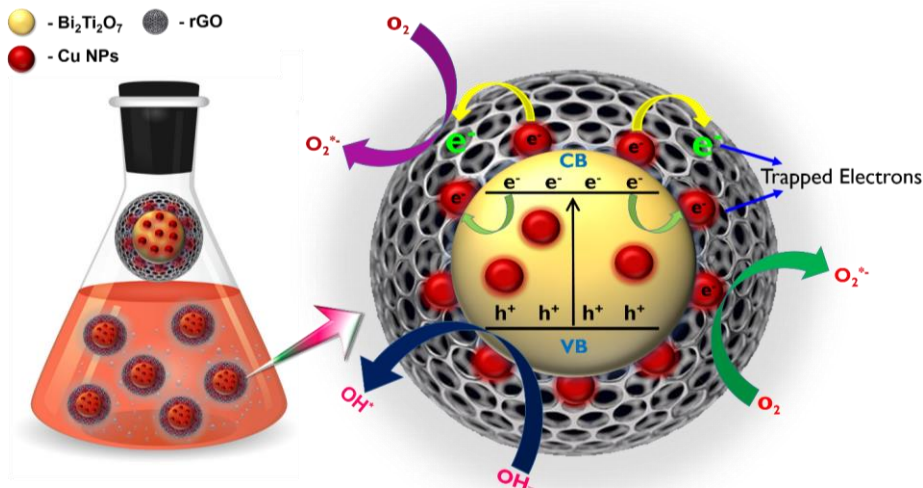
^c *Facultad de Ingeniería y Tecnología, Universidad San Sebastián, Bellavista 7, Santiago 8420524, Chile*

**Corresponding author.*

Phone: +91-0427-2345766, 2345520

Fax No: +91-0427-2345565, 2345124

Graphical Abstract



Abstract

The photoexcited charge carriers trapping is an effective way to generate more number of active species like O₂^{•-} and •OH radicals to oxidize organic carcinogens. In this study, the enhanced trapping of photoexcited charge carriers were successfully obtained by constructing a novel Cu/Bi₂Ti₂O₇/rGO ternary photocatalyst through facile hydrothermal method. In ternary Cu/Bi₂Ti₂O₇/rGO composite Cu nanoparticles and rGO sheets acts as charge carrier trappers and the suppression of e⁻-h⁺ pair recombination was confirmed by PL analysis. The photocatalytic degradation ability of Cu/Bi₂Ti₂O₇/rGO composite was examined by using Rhodamine B and Tetracycline as model carcinogen molecules under visible light irradiation. The Cu/Bi₂Ti₂O₇/rGO composite showed ~8.7 times enhanced photocatalytic degradation ability than P25-TiO₂. The enhancement in photocatalytic ability can be attributed to the synergistic effect between charge carrier trappers (Cu nanoparticles and rGO sheets) and Bi₂Ti₂O₇ nanoparticles. The photocatalytic properties of Cu/Bi₂Ti₂O₇/rGO composite was also analyzed in different reaction parameters, such as pH of reaction solution and initial concentration of both RhB and tetracycline molecules. The

photoexcited charge transfer mechanism in Cu/Bi₂Ti₂O₇/rGO photocatalyst was discussed in detail with the help of UV-Vis DRS and XPS analysis. The active species trapping experiments reveals that O₂^{•-} radical plays major role in carcinogen degradation. The recyclability analysis shows that the Cu/Bi₂Ti₂O₇/rGO photocatalyst is highly stable even after 5 cycle of carcinogen molecule degradation. Therefore, this research designates a promising strategy for higher photoexcited charge carrier trapping photocatalyst design for efficient degradation of carcinogen molecules.

1. Introduction

Clean and fresh water is a chief requirement for entire living organisms, and its obtainability is a predominant problem throughout the habitats. In the near future, availability of fresh water is expected to even more decline due to rapid industrialization and growth of human population. In specific regions, the rapid growth of dyeing and textile industries have instigated serious ecological difficulties^{1,2}. The improper treatment of dye effluents from these industries will contaminate ground water resources and the effluents are directly discharged to other water resources like ponds, rivers and lakes, and their use produces many toxic compounds like carcinogens that have serious effects on humans and other living organisms³. In addition, the extensive use of antibiotics has grabbed an attention because of its possible direct damages to living organisms and agriculture^{4,5}. The antibiotics are usually used to treat bacterial diseases in humans and it promotes growth in animals, huge amount of antibiotics are produced and consumed in day to day life. Among them, tetracycline is the most important antibiotics which is widely used in veterinary and human medicines for disease control and growth promotion due to its high efficiency⁶. But, tetracycline can be easily entered into our aqueous environment because of its poor absorption, lower metabolism, exploitation and overuse. The tetracycline in aqueous environment could cause several direct toxicity effects and potential risks to human health. Over the past decades, these antibiotics and dye effluents are rapidly increasing in water environments and have attracted much attention⁴. To eradicate these challenges, many researches were targeted to deal with carcinogenic condemned water, like biological degradation, chemical reactions and physical absorption. The huge challenges in these methods are their poor efficiency as low concentrations and biochemical rate⁷⁻⁹. While compared with these traditional methods, photocatalytic technology is considered as promising method of degrading carcinogens in aqueous

environment due to its very high mineralization ability, very low energy consumption, no secondary pollution and simple practical application.

The photocatalytic process of semiconductors are primarily depends on the absorption of photons from sun and the separation of photo-excited charge carriers. Unfortunately, the photocatalytic activity of most photocatalyst are still low due to some draw-backs such as the lack of active sites, utilization of photons from sun and the limited fast photoinduced charge carrier recombination¹⁰⁻¹². The catalytic degradation performance of photocatalytic materials can be increased by suppressing the charge carrier recombination on the photocatalyst. It is possible to trap the charge carriers excited in the photocatalytic materials by using noble metals and rGO sheets as charge carrier trappers¹³⁻¹⁵. However, rGO is a single layer of sp² hybridized carbon atoms arranged in a 2D honey comb structure with high surface area, excellent mechanical, thermal and electrical properties. It is an excellent material which excellently supports the metal oxide nanoparticles used in wide range of environmental and energy applications. The combination of rGO with metal oxide nanoparticles results in the novel functional materials with enhanced performance¹⁶⁻¹⁸. Hence, rGO based nanocomposites shows huge enhancements in photocatalytic activity. The excellent surface properties of rGO sheets supports it to accept electrons which are excited on the photocatalytic semiconductors and helps to decline the recombination rate of photoinduced electron-hole pairs. In addition, the π - π conjugation between the aromatic regions of graphene and dyes allows the adsorption of dye molecules on the rGO surface^{10,13,19}. Among several semiconductor photocatalysts, pyrochlore bismuth titanate (Bi₂Ti₂O₇) is one of the new visible light driven photocatalytic material owing to its moderate band gap energy of about 2.88 eV^{20,21}. Due to the considerable band edge positions of Bi₂Ti₂O₇ for oxidation and reduction process to generate active species like hydroxyl and superoxide radicals, Bi₂Ti₂O₇ has been confirmed towards the photocatalytic activity for pollutants removal and water splitting applications^{22,23}. However, there are few practical difficulties while using pristine Bi₂Ti₂O₇ photocatalysts, such as low catalytic activity due to higher recombination rates of photo-excited carriers and it results with low quantum efficiency. In general, it is proved that the binary Bi₂Ti₂O₇/noble metal and Bi₂Ti₂O₇/rGO can efficiently promote the photo-excited charge carrier separation and transfer. A large number of binary semiconductor/noble metal and semiconductor/rGO nanocomposites have been synthesized and attained improvement in photocatalytic efficiency^{15,20}. However, the quantum efficiency of such photocatalytic materials

can be enhanced furthermore by introducing trappers like noble metal and rGO on the pristine $\text{Bi}_2\text{Ti}_2\text{O}_7$ structures as ternary nanocomposites^{24,25}.

In present work, we constructed a novel $\text{Cu}/\text{Bi}_2\text{Ti}_2\text{O}_7/\text{rGO}$ (CBTG) ternary nanocomposite by self-assembly of a 2D rGO sheets with $\text{Cu}/\text{Bi}_2\text{Ti}_2\text{O}_7$ nanocomposite to form ternary nanocomposite. In specific, a simple electrostatic approach has been carried out to synergistically couple rGO with $\text{Cu}/\text{Bi}_2\text{Ti}_2\text{O}_7$ nanocomposite and the properties of thus obtained ternary nanocomposite are examined through several complementary characterization techniques. The main objective of current work is to develop high efficient separation and transmission of photo-induced charge carriers to enhance the reactive species production by photocatalytic materials, and it is achieved by using Cu and rGO as trappers for photo-induced charge carriers. The suppression of charge carriers recombination rate is analyzed and confirmed by PL analysis. The PL analysis of CBTG ternary nanocomposite shows the effective decrement in PL intensity which corresponds to the lower recombination rate of charge carriers. The photocatalytic ability of CBTG ternary nanocomposite to degrade aqueous carcinogens was investigated in detail by using Rhodamine B (RhB) and tetracycline as a target pollutant under visible light irradiation. Furthermore, the possible photocatalytic mechanism and possible degradation pathways of tetracycline and RhB molecules have been examined and proposed in detail. Not only the degradation of carcinogens are enhanced in presence of rGO and Cu as charge carrier trappers in $\text{Bi}_2\text{Ti}_2\text{O}_7$ photocatalyst, cyclic runs indicating higher stability of CBTG composite, highlighting its real time utilization. The novel findings reported in this work are anticipated to assist as an effective strategy in the construction of such high photo-excited charge carrier trapping photocatalyst to develop the catalytic performance towards the degradation of aqueous carcinogens.

2. Experimental Section

2.1 Materials

Graphite flakes, copper sulphate pentahydrate ($\text{CuSO}_4 \cdot 5\text{H}_2\text{O}$), bismuth nitrate pentahydrate ($\text{Bi}(\text{NO}_3)_3 \cdot 5\text{H}_2\text{O}$), titanium(IV) isopropoxide ($\text{Ti}[\text{OCH}(\text{CH}_3)_2]_4$), sodium nitrate (NaNO_3), hydrochloric acid (HCl), potassium permanganate (KMnO_4), sulfuric acid (H_2SO_4), nitric acid (HNO_3), hydrogen peroxide (H_2O_2), cetyltrimethyl ammonium bromide (CTAB), sodium hydroxide (NaOH), hydrazine hydrate ($\text{N}_2\text{H}_4 \cdot \text{H}_2\text{O}$), ethanolamine ($\text{C}_2\text{H}_7\text{NO}$), ammonium hydroxide (NH_4OH), ethanol ($\text{C}_2\text{H}_5\text{OH}$), terephthalic acid, benzoquinone (BQ), isopropyl alcohol

(IPA), triethanolamine (TEOA), tetracycline, rhodamine B and glacial acetic acid (CH_3COOH). All the above mentioned analytical grade chemicals were purchased from Merck Chemical Company and used directly without any further purification.

2.2. Synthesize of photocatalyst

2.2.1 Synthesis of graphene oxide (GO)

GO was prepared by strong oxidation of graphite flakes through modified Hummer's method^{26,27}. In a typical modified hummer's method, graphite flakes, NaNO_3 , and concentrated H_2SO_4 were stirred together at low temperature in an ice bath for 30 min. Subsequently, KMnO_4 was slowly added in a controlled manner to it resulting in the formation of a dark green colored solution. Due to the addition of H_2SO_4 and KMnO_4 the temperature of the solution will increase rapidly but the ice bath was maintained to restrict the temperature as below 20°C . After 5 min of constant stirring the ice bath was removed and the temperature of the reaction solution was increased up to 40°C under stirring for 30 min. The reaction solution converted in a thick paste and then deionized water was added slowly to it. This reaction is exothermic and hence the temperature of the solution is increased. The solution was further slowly heated up to 90°C and constantly maintained at this temperature for 40 min. At that time, deionized water was added followed by dropwise addition of 30% H_2O_2 solution to reduce the presence of excess KMnO_4 . Now, the color of the reaction solution was changed from dark brown to yellow. The mixture was kept under constant stirring for some time and filtered out from the hot acidic solvent. The obtained filtered block like material was washed several times with warm water. Then the recovered material was well dispersed in cold water by sonication followed by centrifugation several times. The separated black colored material was dried and used for further characterization and composite preparation.

2.2.2 Synthesize of pristine Cu

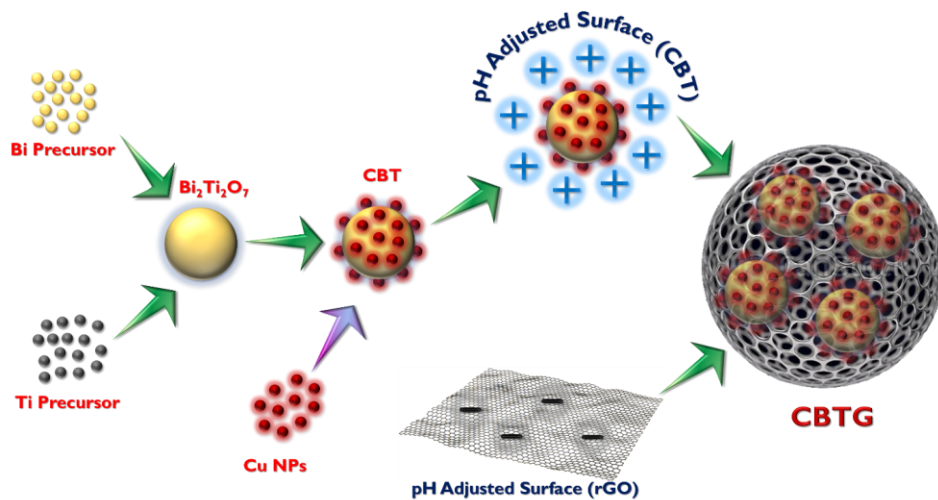
The Cu nanoparticles were synthesized via typical experimental procedure, 0.01 M of $\text{CuSO}_4 \cdot 5\text{H}_2\text{O}$ were well dissolved in 50 mL of deionized water and stirred for 30 min to obtain homogeneous solution. Then, 0.1 M NaOH aqueous solution was added quickly until pH of the solution reaches 10. Finally, 1 ml of M of hydrazine hydrate was added drop wise into the solution under constant stirring. The reduction reaction was done in single step under reflux treatment at

80 °C for 1 h. The shiny brown colored particles was precipitated and it was separated by centrifugation and washed using deionized water and anhydrous ethanol several times. The obtained final shiny brown product was collected and dried in vacuum at 80 °C for 6 h.

2.2.3 Synthesize of pristine Bi₂Ti₂O₇ and Binary CBT nanocomposite

The Pristine Bi₂Ti₂O₇ particles were synthesized through simple co-precipitation method. Initially, Titanium isopropoxide and bismuth nitrate stock solutions were prepared for Bi₂Ti₂O₇ synthesize. To produce stock solution A, 0.1 M of Titanium isopropoxide was hydrolyzed in deionized water to form a white precipitate of titanium hydroxide/oxohydroxide. The obtained white precipitate was dissolved in concentrated nitric acid with sonication for 10 min in closed container followed by the addition of deionized water to maintain an acid concentration at 1 M. Bismuth nitrate stock solution was prepared by dissolving 0.1 M of solid bismuth nitrate in nitric acid of 1 M concentration and labeled as solution B. Equal volumes of solution A and solution B is well mixed by stirring at 400 rpm for 15 min followed by the addition of strong ammonium hydroxide solution until the pH of the solution reaches 10. The formation of metal hydroxides in the form of precipitated was observed. The obtained precipitated was collected and washed several times with deionized water and ethanol and dried in hot air oven at 120 °C. The obtained dried material was finely grind using mortar and calcinated at 600 °C for 6 h. The binary CBT nanocomposite was prepared by adding 1 M of Cu nanoparticles after the addition of strong ammonium hydroxide solution and subsequent washing and heating process was done as same as the above reaction process

2.2.4 Synthesize of ternary CBTG capsules



Scheme. 1: Synthesize of CBTG capsules

The ternary CBTG capsules were prepared by a simple hydrothermal assisted self-assembly process (Scheme. 1). The as-prepared CBT nanocomposite was well dispersed in 150 ml of deionized water by constant sonication until uniform dispersion occurs. The surface of CBT composite was tuned as positive by adding acetic acid (drop wise) and the pH of the suspension is maintained at ~3. GO was well dispersed in deionized water by sonication and the pH of GO dispersion is maintained at ~8 using ammonium hydroxide. The basic medium results in the deprotonation of the carboxylate groups on the GO surface, making it negatively charged. Then 0.5 wt% of GO suspension (with respect to CBT) was added to the surface-tuned CBT dispersion. The mixing of positive and negative charged suspensions causes an instant flocculation due to self-assembly of oppositely charged components and also results in a transparent supernatant¹⁵. The obtained flocculated matrix with supernatant was quickly transferred to an autoclave and maintained at 160 °C for 4 h and after that the reaction mixture was allowed to cool slowly until it attains room temperature. The hydrothermally treated flocculated matrix was well centrifuged to separate supernatant, followed by drying and annealing of the sample at 120 °C for 6 h and the obtained black sample is labeled as CBTG.

2.3 Characterization techniques

The crystalline phase and structure of as-synthesized photocatalyst was examined by powder X-ray diffraction (XRD) powder X-ray diffraction using a (Rigaku Miniflex X-ray diffractometer equipped with Cu K α ($\lambda = 1.54 \text{ \AA}$) radiation source operating at 40 kV with 30 mA. The X-ray diffraction patterns were recorded for 15 min with continual scanning rate of 4° min^{-1} in the wide range of $2\theta = 20\text{--}80^\circ$. The chemical states of as-synthesized photocatalyst was analyzed by X-ray photoelectron spectroscopy (XPS) measurement was analyzed by Krotas analytical Instrument, Shimadzu Corporation, ESCA 3400, Japan, with Dual Mg/Al anodes and operating voltage at 12 kV with 25 mA under ultra-high vacuum condition. The functional groups in catalytic materials are analyzed by recording Fourier transform infrared (FTIR) spectra using Bruker Tensor 27 spectrophotometer in the range of $4000\text{--}400 \text{ cm}^{-1}$ at solid KBr phase. The morphological characteristics of as synthesized nanostructures were characterized by field emission scanning electron microscope (SEM, Zeiss 18 Evaluation) and transmission electron microscopy (Jeol/JEM 2100). The high resolution transmission electron microscopy (HR-TEM) was performed by LaB $_6$ electron gun with an acceleration voltage of 200 kV and was analyzed by digital micrograph software. The optical characteristics of as-synthesized catalyst was analyzed by UV-Vis diffuse reflectance spectrometer (DRS) (SHIMADZU-UV 1800) in the wavelength range of about $\lambda=200\text{--}800 \text{ nm}$. The photoluminescence (PL) properties were examined by with Perkin Elmer LS-45 fluorescence spectrophotometer at room temperature (excited at $\lambda = 330 \text{ nm}$).

2.4. Photocatalytic performance analysis and reactive species identification

The photocatalytic degradation ability of as-synthesized samples were evaluated by the photocatalytic degradation of carcinogens like tetracycline and RhB in aqueous solution under visible light irradiation. In a typical photodegradation process, 0.5 g of catalyst was added to 100 mL of 50 mg of pollutant solution. The catalytic reaction mixture was stirred in the dark for 30 min to attain an adsorption–desorption equilibrium between catalyst particles and pollutant molecules before visible light illumination. Then the reaction solution was irradiated by the visible light using Xenon lamp with 100 W. The photocatalytic reaction suspension was stirred continuously during photocatalytic degradation process. In regular periodic intervals of irradiation, about 2.5 mL sample solution was collected, centrifuged and then analyzed through UV-Vis

spectrometer. In order to find the stability and reusability of photocatalyst the several cycles of pollutant degrading were implemented. In addition, the reactive species responsible for photocatalytic degradation of pollutants were effectively determined by the trapping experiments. Superoxide radicals ($O_2^{\bullet-}$), hydroxyl radicals ($\cdot OH$) and holes (h^+) were examined by adding BQ ($O_2^{\bullet-}$ -suppressor), IPA ($\cdot OH$ -suppressor) and TEOA (h^+ -suppressor), all the above substances were taken in the concentration of 0.1 mmol/100mL¹¹. The procedures of active species trapping experiment was similar to the above discussed photocatalytic pollutant degradation process. The suppressors were added separately into the aqueous tetracycline and RhB solution before the addition of catalyst.

2.5. Analysis of hydroxyl radical productions

The production of hydroxyl radicals by synthesized nanostructures were analyzed by employing terephthalic acid (TA) as probe molecule. The reaction process between terephthalic acid (TA) and hydroxyl radicals occurs to produce 2-hydroxyterephthalic acid (HTA) (a fluorescent molecule)²⁸. In this experiment, 0.1 mM of TA solution is dissolved in 100 ml of deionized water. To this, 0.5 g of catalyst was well dispersed by sonication in dark for 30 min. Then, the reaction solution was exposed to xenon lamp. The photon-irradiated solution in the presence of catalyst was collected and centrifuged to remove the catalyst and the PL spectrum of solution was recorded at excitation wavelength of 315 nm. The PL spectrum of solution was recorded periodically with regular interval of time.

3. Results and discussion

3.1 Structural Analysis

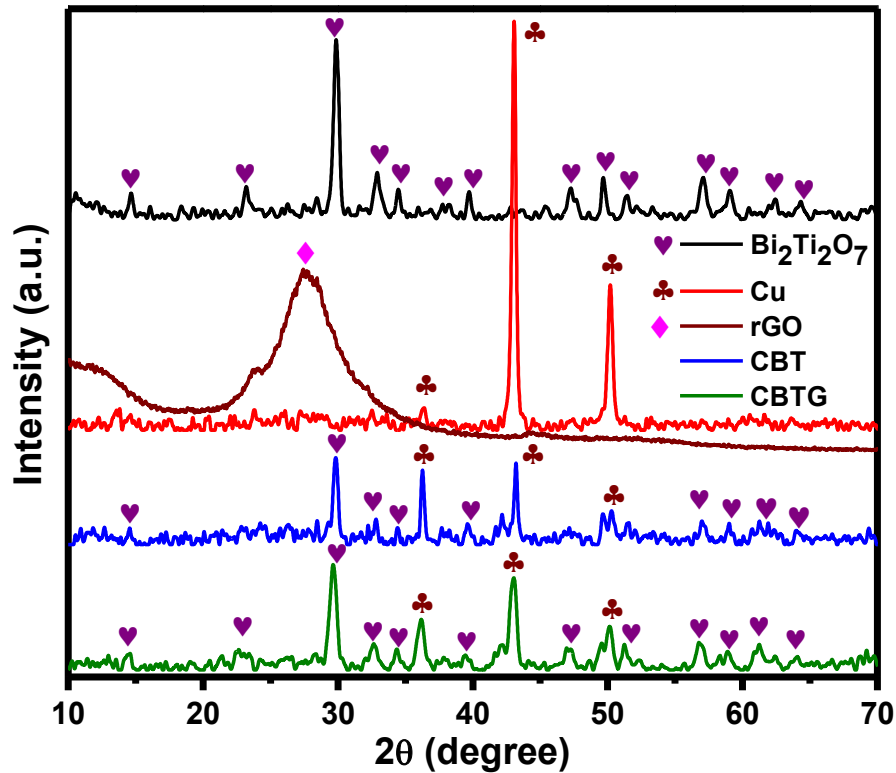


Fig. 1: XRD spectra of as synthesized pure and composite nanostructures.

The crystalline phase and structural analysis of as synthesized rGO, Cu, $\text{Bi}_2\text{Ti}_2\text{O}_7$, CBT and CBTG nanostructures were carried out by XRD analysis (Fig. 1). The strong peaks in XRD diffractogram of as-synthesized pure and composite nanostructures shows that the obtained products are highly crystallized in nature. In Fig. 1, the typical XRD diffractograms of pure Cu and $\text{Bi}_2\text{Ti}_2\text{O}_7$ nanostructures where shown, all diffraction peaks of $\text{Bi}_2\text{Ti}_2\text{O}_7$ can be represented to its pure cubic phase. The characteristic peaks at $2\theta = 14.97^\circ, 30.2^\circ, 32.32^\circ, 34.63^\circ, 38.37^\circ, 48.26^\circ, 52.53^\circ, 58.23^\circ$ and 62.35° can be indexed to (222), (444), (642), (800), (662), (1042), (1062), (1244) and (888) planes of cubic phase of $\text{Bi}_2\text{Ti}_2\text{O}_7$ (JCPDS no. 32- 0118)^{4,22,23}. The XRD

diffraction pattern of Pure Cu nanoparticles shows a typical diffraction peaks at 36.35° , 43.09° and 50.20° can be indexed to (110), (111) and (200) planes of cubic Cu nanoparticles (JCPDS no. 04-0836)²⁹⁻³¹. The diffraction patterns of the CBT nanocomposite shows that all the characteristic diffraction peaks are in good arrangement with the cubic Cu and cubic $\text{Bi}_2\text{Ti}_2\text{O}_7$ crystallite phases. These results exposed that binary nanocomposite is well composition of Cu and $\text{Bi}_2\text{Ti}_2\text{O}_7$ nanoparticles. In Fig. 1, XRD pattern of as synthesized graphite oxide shows a strong diffraction peak at $2\theta = 10.3^\circ$, corresponding to the (001) plane of graphite oxide. In the XRD pattern of RGO nanosheets, the peak at $2\theta = 10.3^\circ$ was disappeared that confirms that GO is successfully reduced into rGO nanosheets¹⁵. The presence of Cu, $\text{Bi}_2\text{Ti}_2\text{O}_7$ and rGO XRD peaks in nanocomposite confirms the well formation of ternary nanocomposite. In CBTG Nanocomposite the characteristic peak of rGO was not clearly visible. It is due to the merging of $\text{Bi}_2\text{Ti}_2\text{O}_7$ peak with characteristic peak of rGO and also due to lower mass percentage composition (5%) of rGO in ternary nanocomposite. The XRD diffraction peaks on ternary nanocomposite is significantly widened this is due to the formation of small sized particles as a composition of ternary nanocomposite. The d-spacing of Cu and $\text{Bi}_2\text{Ti}_2\text{O}_7$ was calculated as 0.21 nm and 0.298 nm for pristine Cu and pristine $\text{Bi}_2\text{Ti}_2\text{O}_7$ from there high intense peak at $2\theta = 30.2^\circ$ and 43.09° respectively by using Bragg's law^{32,33}. The obtained d-spacing values were correlated with HRTEM results of respective pristine nanostructures.

3.2 FT-IR Analysis

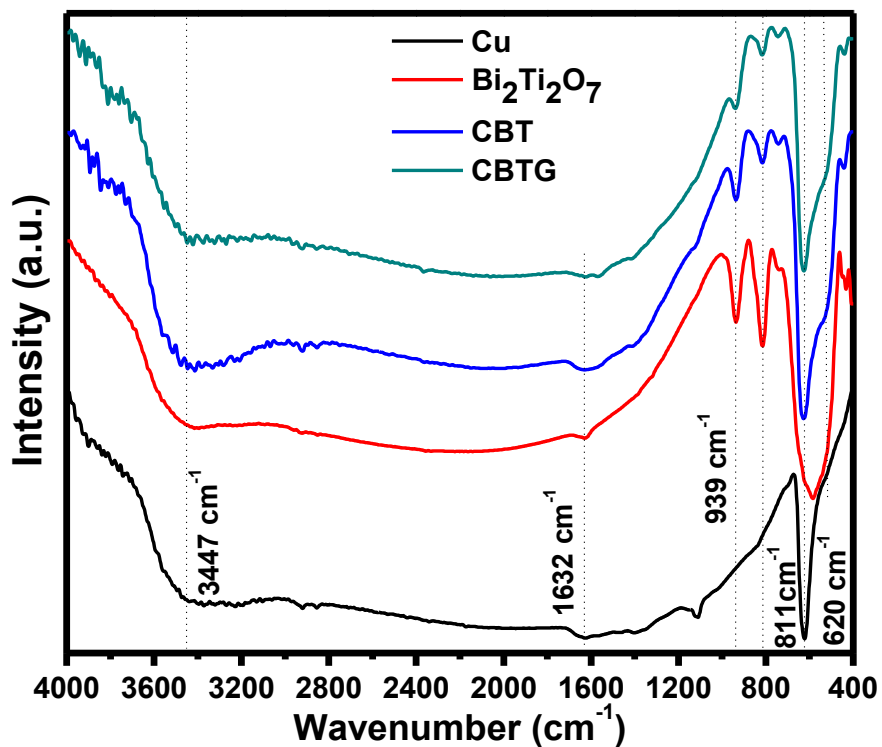


Fig. 2: FT-IR spectrographs of as-synthesized nanostructures

The chemistry of all the functional groups and surface characteristics of as-prepared pristine Cu, Pristine Bi₂Ti₂O₇, CBT and CBTG, were further investigated and clarified using FT-IR spectroscopy and the obtained results were shown in Fig. 2. The catalytic oxidation of organic dyes and reagents are highly governed by the functional groups presented on the surface of catalytic materials. The surface behavior and surface characteristics of the catalytic materials are highly affected by the carboxyl functional groups¹². The FT-IR spectrum of Pristine Bi₂Ti₂O₇ shows the strong absorption peak between 450 cm⁻¹ and 750 cm⁻¹, it confirms the formation of metal-oxygen bonding such as Bi-O-Bi and Ti-O-Ti. The stretching peak of -OH bond vibration, stretching vibration peaks (1000–800 cm⁻¹) of C-O and C-O-C bonds as well as the symmetric stretching vibration peak (1384 cm⁻¹) of O-C-O still can be observed^{34,35}. The FTIR spectrograph

of Cu nanoparticles and all other as synthesized nanostructures shows the wider absorption peak at 3400 to 3800 cm^{-1} , it corresponds to the N-H stretching vibration of amino groups and the hydroxyl stretching vibrations of water molecules absorbed on the surface of nanoparticles¹⁰. Besides, no peak of Cu nanoparticles are observed in FTIR analysis because Cu is inactive for infrared spectra. In the case of CBTG ternary nanocomposite, the peaks at 939 and 811 cm^{-1} are observed with less intense than the pristine nanostructures it is due to the binding of pristine nanoparticles with the surface of rGO¹¹. The bands at 1632 cm^{-1} is developed due to the metal-O-C vibration of Bi and Ti atoms, they are suggesting the effective atomic interaction between Bi and Ti with carbon atoms of rGO¹⁵. In addition, the absorption peak signals in the range between 450 and 700 cm^{-1} can be attributed to the metal-oxygen bonding such as Ti-O-Ti and Bi-O-Bi bonding resulting on the surface of rGO¹⁵. The most of the oxidized functional groups are disappeared in CBTG nanocomposites and the presence of metal-oxygen bonding groups shows the successful incorporation of both $\text{Bi}_2\text{Ti}_2\text{O}_7$ and Cu nanoparticles on the surface of rGO sheets.

3.3 Morphological characterization and elemental analysis

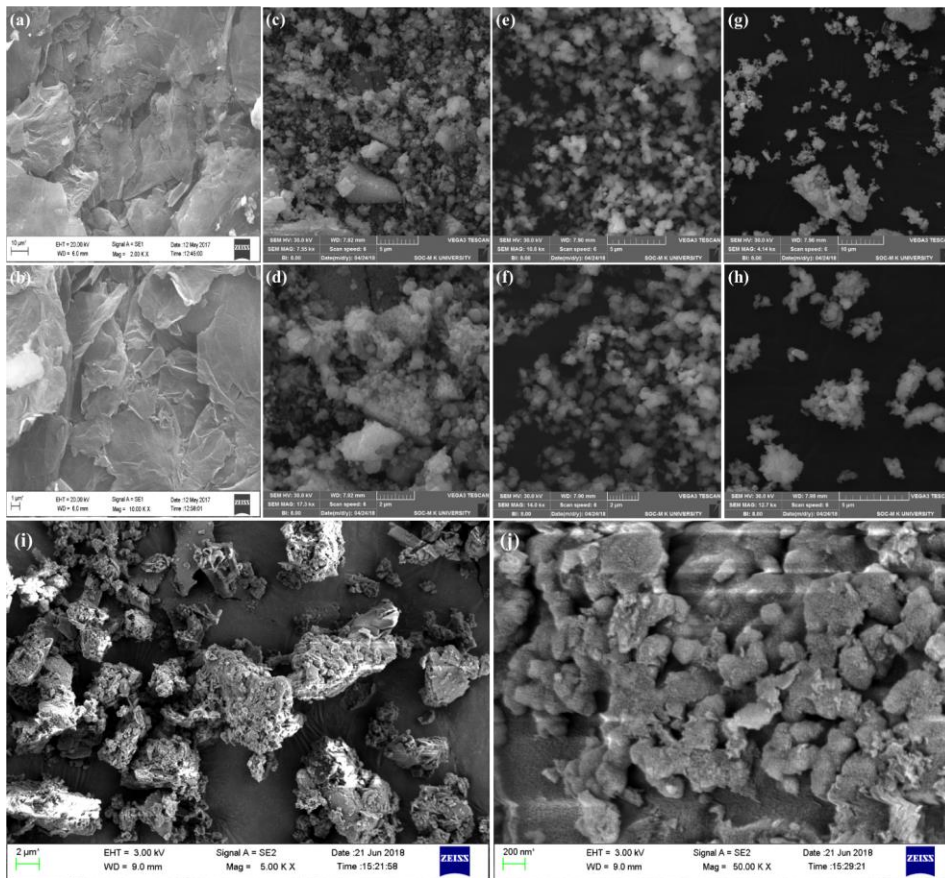


Fig. 3: SEM micro graphs of (a-b) rGO, (c-d) Pristine $\text{Bi}_2\text{Ti}_2\text{O}_7$, (e-f) Pristine Cu, (g-h) CBT

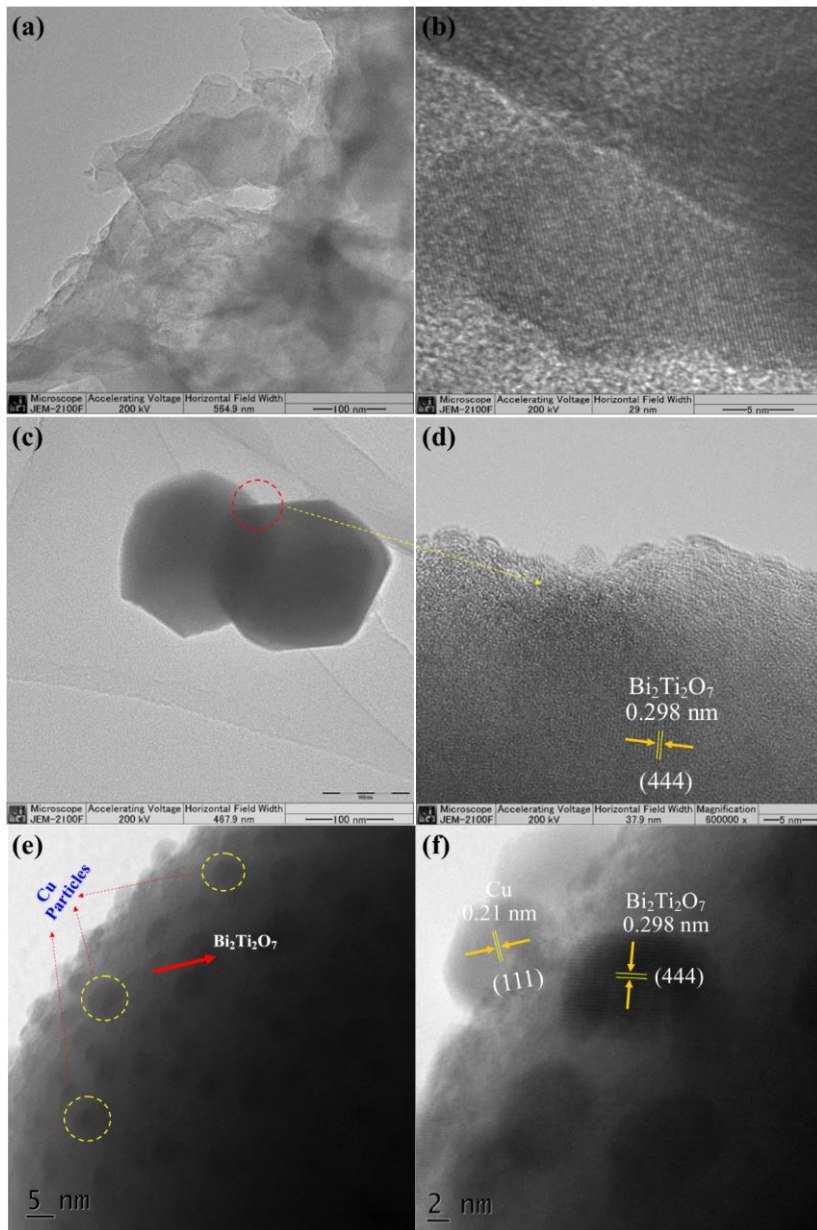


Fig. 4: HR-TEM images of (a,b) rGO, (c,d) Pristine $\text{Bi}_2\text{Ti}_2\text{O}_7$, (e,f) CBT

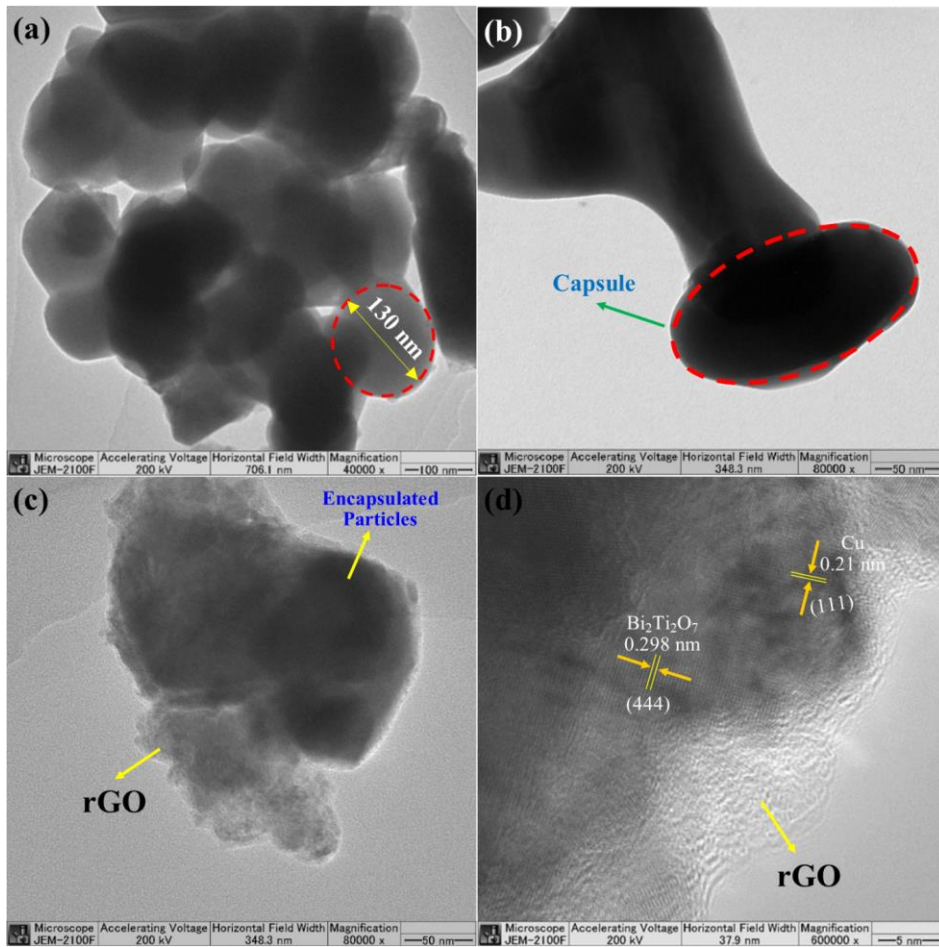


Fig. 5: HRTEM images of CBTG capsules

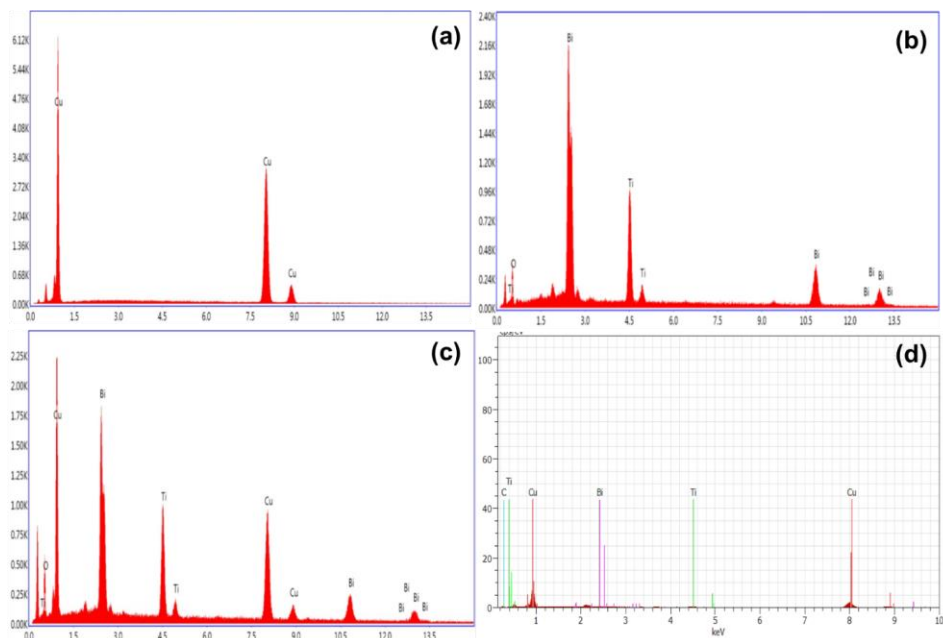


Fig. 6: EDX analysis graph of (a) Pristine Cu, (b) Pristine $\text{Bi}_2\text{Ti}_2\text{O}_7$, (c) binary CBT and (d) ternary CBTG capsules

The detailed morphological properties of as prepared pristine Cu, $\text{Bi}_2\text{Ti}_2\text{O}_7$, CBT and CBTG capsules were revealed by using SEM and High resolution TEM (HR-TEM) characterisation techniques. The formation of crumpled sheet like rGO with folding and wrinkles on its surface were obtained in both SEM and HR-TEM images as seen in **Fig. 3** and **Fig. 4**. The SEM images of the pristine $\text{Bi}_2\text{Ti}_2\text{O}_7$ as presented in Fig. 3c and 3d reveals the formation of spherical shaped nanoparticles with uniform size and homogeneous agglomeration. The pristine Cu nanoparticles shown in **Fig. 3e and 3f** are found to have a spherical structure with freely dispersed with each other this freely dispersing ability of Cu nanoparticles will results with the well attachment of Cu nanoparticles with $\text{Bi}_2\text{Ti}_2\text{O}_7$ nanostructures and shown in **fig. 3(g,h)**. The SEM and TEM of CBTG capsules, as shown in Fig 3i and 3j respectively revealed the formation of well agglomerated spherical and ellipsoidal shaped CBTG capsules with size of about ~150 nm. Formation of such inorganic oxide with graphene or graphene-like material has been also reported

Commented [EG1]: I think that this sentence has to be re-written, as in the current form doesn't makes much sense.

in similar studies.^{13,15} The difference between the TEM images of Cu and Bi₂Ti₂O₇ nanoparticles with CBTG capsules are presented in Fig. 4 and Fig. 5. The size of CBTG capsules is comparatively larger than the pristine Cu and Bi₂Ti₂O₇ particles due to the binding between the Cu and Bi₂Ti₂O₇ nanostructures with the rGO sheets. Furthermore, the results showed that the Cu nanoparticles and the pyrochlore Bi₂Ti₂O₇ nanostructures are well encapsulated in the rGO nanosheets. Such a tight contact between the surface of Cu and Bi₂Ti₂O₇ nanostructures with the rGO sheets is desired for the reasons introduced and is expected to support the photocatalysis process. The encapsulation of the nanoparticles is mainly due to the electrostatic interaction between the nanoparticles and rGO sheets³⁶. The surface contact between nanoparticles and rGO sheets was highly increased due to the enrichment of surface charges of pristine nanoparticles and rGO sheets during the synthesis. This obtained results indicated that electrostatic self-assembly approach assisted the encapsulation of Cu and Bi₂Ti₂O₇ nanostructures with rGO sheets. During the electrostatic self-assembly process, the wrapping of the rGO sheets can be expected to continue until the attainment of charge neutralization between the positively charged CBT surface and the negatively charged rGO surface^{15,37}. If the rGO loading is higher, the excess rGO sheets are expected to remain in the reaction solution without wrapping around the nanostructures, due to the lack of positively charged CBT surface. From the HRTEM images of pristine Bi₂Ti₂O₇, CBT and CBTG capsules the presence of Cu and Bi₂Ti₂O₇ nanoparticles can be clearly identified from the respective lattice fringes. The fringe lines with spacing of about 0.298 nm is due to the formation of cubic Bi₂Ti₂O₇ particles and that of 0.21 nm corresponds to the Cu nanoparticles. The purity of as-prepared pristine nanomaterials and nanocomposites were further confirmed by energy dispersive X-ray analysis (EDX) and the results shows that the materials were highly pure in nature. The presence of Cu and Bi₂Ti₂O₇ particles in CBTG capsules were confirmed by using EDX analysis as presented in **Fig. 6**.

3.4 Chemical state analysis

Commented [EG2]: Maybe a reference here

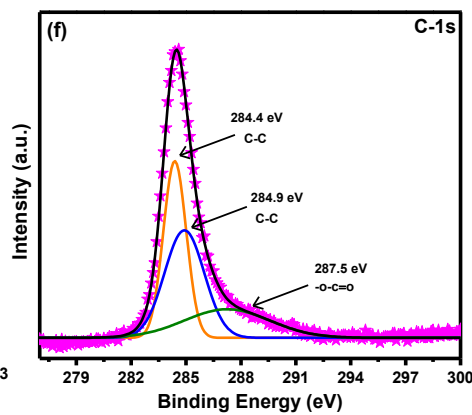
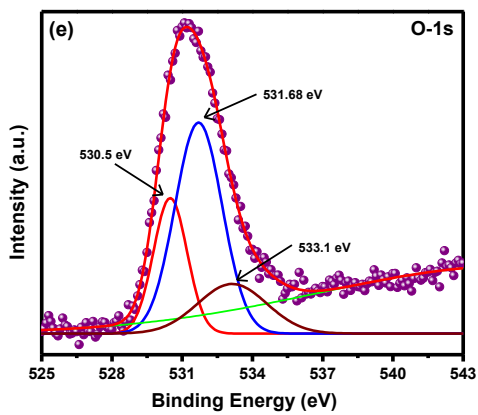
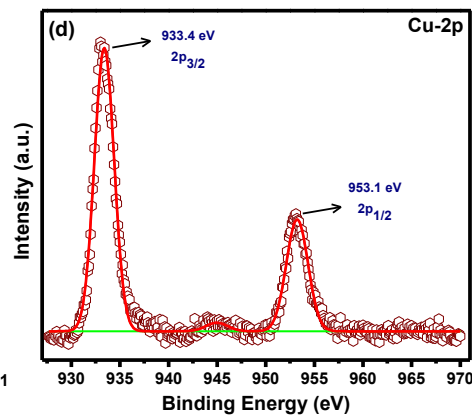
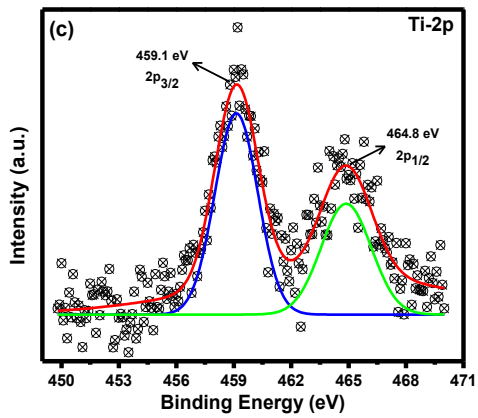
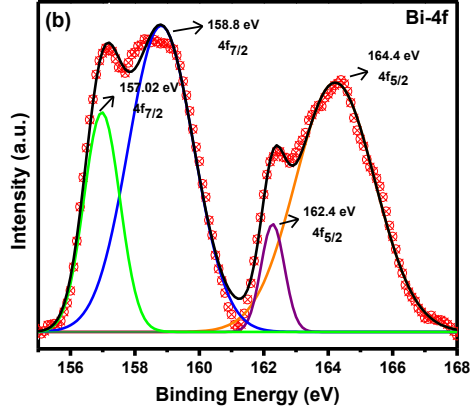
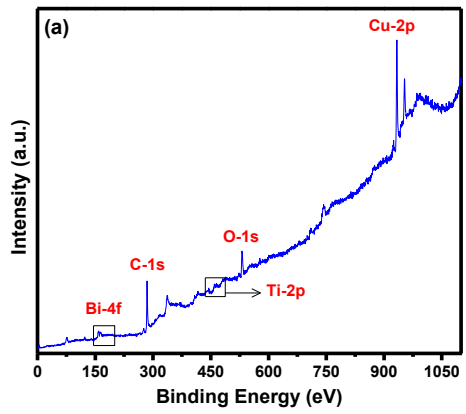


Fig. 7: XPS spectra of CBTG: (a) survey spectra, (b) Bi-4f, (c) Ti-2p, (d) Cu-2p, (e) O-1s, (f) C-1s.

In order to understand the valence state and the surface chemical composition of the CBTG capsules, XPS technique is used and the survey spectrum of CBTG sample was displayed at Fig. 7a. The survey spectra introduce the presence of Cu, Bi, Ti, O and C elements. The high-resolution XPS analysis of the Cu-2p, Bi-4f, Ti-2p, O-1s and C-1s for this CBTG capsule was also studied and is represented in Fig. 7(b-f). The high resolution XPS spectra of Bi-4f region shown in Fig. 7b is dominated by Bi-4f_{7/2} and Bi-4f_{5/2} components with the peaks observed at 157.02 and 158.08 eV for Bi-4f_{7/2} whereas, 162.4 and 164.4 eV for Bi-4f_{5/2}^{38,39}. The peaks at 158.8 and 164.4 eV with little peak shift of about 1 eV from the previously reported XPS analysis of pure Bi₂Ti₂O₇, can be attributed to the interaction between pyrochlore bismuth titanate and rGO sheets. The binding energy of the Bi-4f_{7/2} component 157.02 and 158.08 eV has an intermediate value between bismuth metal (156.85 eV) and typical Bi(III) oxides (159.0 eV to 159.8 eV)⁴. In Fig. 7, two peaks were observed at the binding energies of about 459.2, 464.8 eV, which are attributed to the Ti-2p_{1/2} and Ti-2p_{3/2} states^{40,41}. A characteristic Ti-2p spin-orbit splitting of 5.6 eV ascribes to a normal state of Ti⁴⁺ in CBTG capsules. The peak at 464.8 eV is also due to the partially overlapped Ti-2p_{1/2} and Bi-4d_{3/2} peaks. The XPS spectra of Cu-2p is illustrated in Fig. 7d with two peaks at 933.4 eV and 953.1 eV for Cu-2p_{3/2} and Cu-2p_{1/2}, respectively, with the splitting of about 20 eV, which evidence towards the production of metallic Cu by reducing CuSO₄ during hydrothermal process. The high resolution O-1s spectra of CBTG capsules is presented in Fig. 7e. The two peaks identified at 530.5 eV and 531.68 eV are attributed to Bi-O lattice oxygen and Ti-O lattice oxygen bonds, respectively. More specifically, the existence of the peak at 531.05 eV is credited to the surface adsorbed -OH group and chemisorbed oxygen-containing species and may be in favor of the enhancement in photocatalytic properties^{15,42}. The interface between CBT and rGO was further probed by high resolution XPS analysis of element C1s and is presented in Fig. 7f. The deconvolution of the obtained C-1s XPS spectra shows two peaks at 284.4 eV and 287.5 eV corresponding to graphitic -C-C and -O-C=O functionalities respectively. The -O-C=O functionalities are formed during the strong oxidation of the graphene sheets using modified hummers method³⁷. The deconvoluted peak presented between 286 eV to 289 eV is comparatively less intense than that of GO. The significant decrement in oxygenated carbon species in CBTG capsules are due to the reduction of GO in to rGO during the hydrothermal reaction. This results

Commented [EG3]: Maybe to analyse the credentials here

revealed that the GO is considerably reduced after the hydrothermal reaction process to form rGO and its composite with CBT. The existence of $-O-C=O$ shows the formation of metal oxygen binding as $Ti-O-C=O$ through the reduction of $Ti-OH$ in $Bi_2Ti_2O_7$ and $COOH$ groups at surface of the graphene¹⁵.

3.5 Valence band analysis

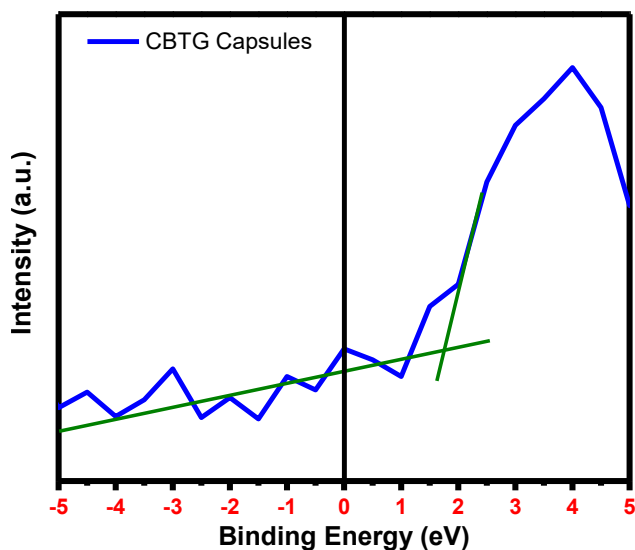


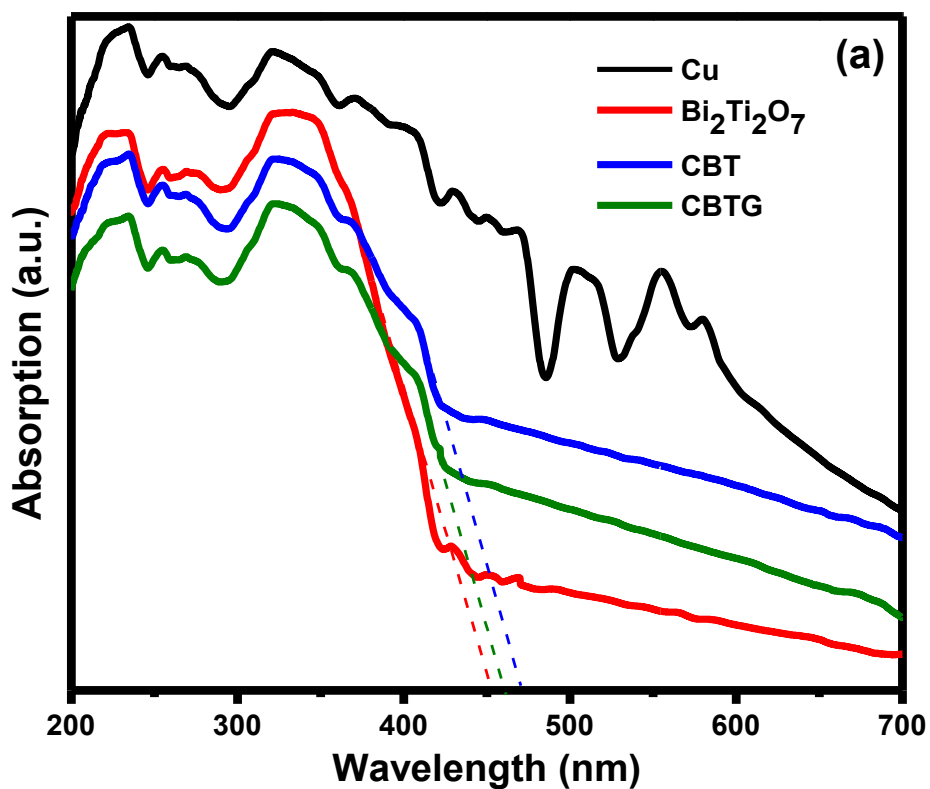
Fig. 8: XPS valence band spectra of CBTG capsules

The energy band edge positioning is the predominant parameter for developing excellent photocatalytic materials. The adjustment of the band edges towards the desired potential levels will effectively enhance the light harvesting efficiency and will promote the utilization of charge carriers for oxidation and reduction cycles during photocatalytic activity¹⁰. The band edge adjustments can be greatly succeeded by introducing new energy levels and narrowing the band gap energy during nanocomposite formation⁴³. The introduction of metal nanoparticles and graphene sheets can effectively bend the band edges of materials due to their band energy levels^{44,45}. The band edges of the materials can be effectively determined by using XPS analysis and the XPS valence band spectra of CBTG capsules were shown in **Fig. 8**. The extrapolated dominant edge of the valence band spectra can provide the valence band value of material and it

Commented [EG4]: Maybe here to mention a few numbers in terms of band energy of graphene and nps

was found to be 1.75 eV for the CBTG capsules. In previous research studies, the valence band edge of $\text{Bi}_2\text{Ti}_2\text{O}_7$ was found to be 1.92 eV which is 0.17 eV higher than our CBTG capsules. The obtained valence band potential of the CBTG capsules is higher than the redox potential of $\text{O}_2/\text{H}_2\text{O}$ (1.23 eV) and hence CBTG capsules can effectively splits H_2O molecules to generate active species¹². The shifting of the valence band towards conduction band could decreases the band separation energy thereby it results with the improved production of active species during photocatalytic process.

3.6 Optical Investigation



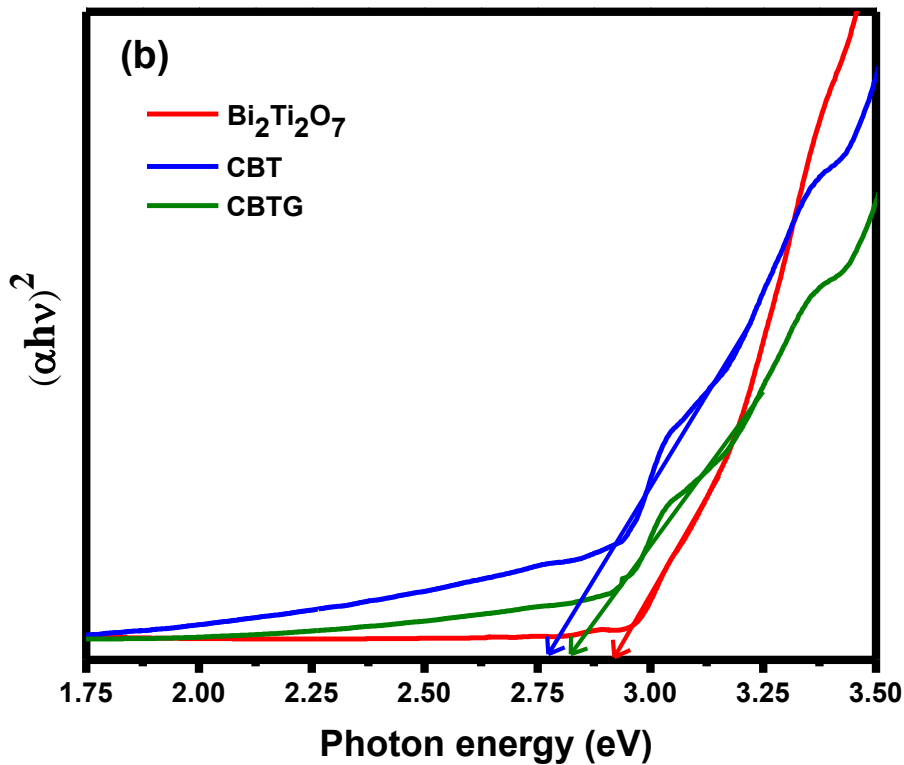


Fig. 9: (a) UV-Vis DRS graph (b) Tauc plot of as synthesized nanostructures

The photon absorbing ability of a semiconductor is inseparably linked to its electronic structure and it is considered as the predominant factor responsible for its photocatalytic activity¹⁴. The optical properties of the as-synthesized Cu, Bi₂Ti₂O₇, CBT and CBTG nanostructures were characterized by UV-Vis DRS spectroscopy and is presented in Fig. 9. From Fig. 9a, it is extracted that all the as prepared nanostructures show strong absorbance in the visible light region. Predominantly, the absorption spectra of CBT and CBTG capsules shows distinctly improved visible-light absorption compared to other photocatalysts. While comparing with pristine Bi₂Ti₂O₇ ternary nanocomposite showed a shift towards the red on photon absorption edge at 460 nm. The photon absorption band edges of Bi₂Ti₂O₇ and CBT were found to be 452 and 470 nm respectively. The characteristics absorption peaks of Cu nanoparticles were observed around 570 nm, this could be attributed to the surface plasmon resonance occurred in the conduction bands of Cu

Commented [EG5]: Maybe mention few of them

nanoparticles. The surface plasmon resonance effect is due to the generation of strong electromagnetic fields at the surface of metal particles when a wavelength of incident light coincident with surface plasmonic optical absorption. In previous research endeavors, the surface plasmon resonance of Cu nanoparticles was in the absorption range between 550-590 nm because free electrons present in the conduction bands were persuaded and oscillated by photons⁴⁶. In addition to that, another optical absorption peak at 500 nm was observed for the prepared Cu nanoparticles. This variation of optical absorption can be ascribed due to the negligible difference in geometry from particles to sheets and it will affect the scattering of photons to diverse extent⁴⁷. When Cu nanoparticles composites with the metal oxides it enhances the absorption of photons in visible region due to surface plasmon resonance. The improvement in photon absorption ability of CBT is due to either improvement in charge transfer from electrons excited from plasmon resonance in Cu to conduction band of Bi₂Ti₂O₇ or due to the enhancement of the local electric field, where electron-hole pair generation rate becomes much faster⁴⁸. When the Cu and Bi₂Ti₂O₇ nanostructures were encapsulated with rGO, the absorption spectra of CBTG capsules shows very close absorption edge with CBT nanocomposite. The encapsulation of pristine Cu and Bi₂Ti₂O₇ nanostructures slightly decreases the light absorption ability, this may be due to the complete encapsulation of nanostructures within the rGO sheets³⁶. But the composition of CBT and the encapsulation of these nanostructures with rGO shows better photonic absorption than the pristine Bi₂Ti₂O₇. According to the above observation, it can extracted that the CBTG capsules can absorb visible light on a more effective way. In general, the photon absorption ability of photocatalyst is often associated with its band gap energy. The band gap energy of the as-prepared nanostructures can be determined by using Tauc plot¹¹. The plots of $(ahv)^2$ vs hv of as prepared samples are presented in Fig. 9b. The intercepts of extrapolated linear line of the curves at x-axis allow the calculation of the band gap energies of Bi₂Ti₂O₇, CBT and CBTG photocatalysts. The band gap energies of pristine Bi₂Ti₂O₇, CBT and CBTG was found to be 2.88, 2.75 and 2.79 eV, respectively, suggesting that the CBT and CBTG photocatalysis does not have huge difference in photon absorption ability but decrement in recombination rate of (e⁻ - h⁺) will effectively increase the photocatalytic ability and it is discussed in next section.

Commented [EG6]: Maybe a reference here

3.7 PL analysis

Fig. 10: Photoluminescence spectra of as-synthesized $\text{Bi}_2\text{Ti}_2\text{O}_7$, CBT nanoparticles and CBTG nanocapsules.

The photocatalytic performance of nanostructures was closely associated to the separation and recombination dynamics of photo-induced electrons and holes. The PL spectra of the as-prepared nanostructures as well as the CBTG capsules can provide the information about their photo-induced electron-hole (e^-h^+) pair separation efficiency¹². The (e^-h^+) pair recombination rate can be directly measured by the intensity of the PL spectrum of the respective materials. If the PL spectrum of the nanostructure is more intense, then the recombination of (e^-h^+) pair is expected to be higher. Otherwise, the lower PL intensity indicates that the more photoexcited electrons were trapped and firmly transferred through the interface of catalyst¹⁰. As presented in Fig. 10, a strong and wide emission band was observed at 478 nm in the PL spectra of $\text{Bi}_2\text{Ti}_2\text{O}_7$ it is correspond to the bound excitons⁴. When the Cu nanoparticles are incorporated with pristine $\text{Bi}_2\text{Ti}_2\text{O}_7$, the PL intensity was highly decreased. It is due to the existence of Schottky barriers at $\text{Bi}_2\text{Ti}_2\text{O}_7$ and Cu interface, the Cu nanoparticles will acts as electron trap to preventing recombination of (e^-h^+) pairs^{13,49}. The PL intensity was decreased further when rGO is introduced with the binary composite. The reason for the decrement in PL intensity is due to the rapid delocalization of photo-excited electrons to the rGO sheets and reducing the (e^-h^+) pair recombination probability¹⁶. In addition, little red-shifts were observed in the PL spectra, after incorporating rGO with the CBT nanocomposite. It may be attributed to molecular conjugation between $\text{Bi}_2\text{Ti}_2\text{O}_7$ with Cu nanoparticles and rGO sheets. These results clearly state that the as-prepared CBTG capsules not only enhances the light absorption ability, but also constrains the photo induced (e^-h^+) pair recombination which is more responsible for enhancing its photocatalytic performance.

3.8 Photocatalytic examination and degradation kinetics of carcinogens

Commented [EG7]: Is there a relative study to confirm this?

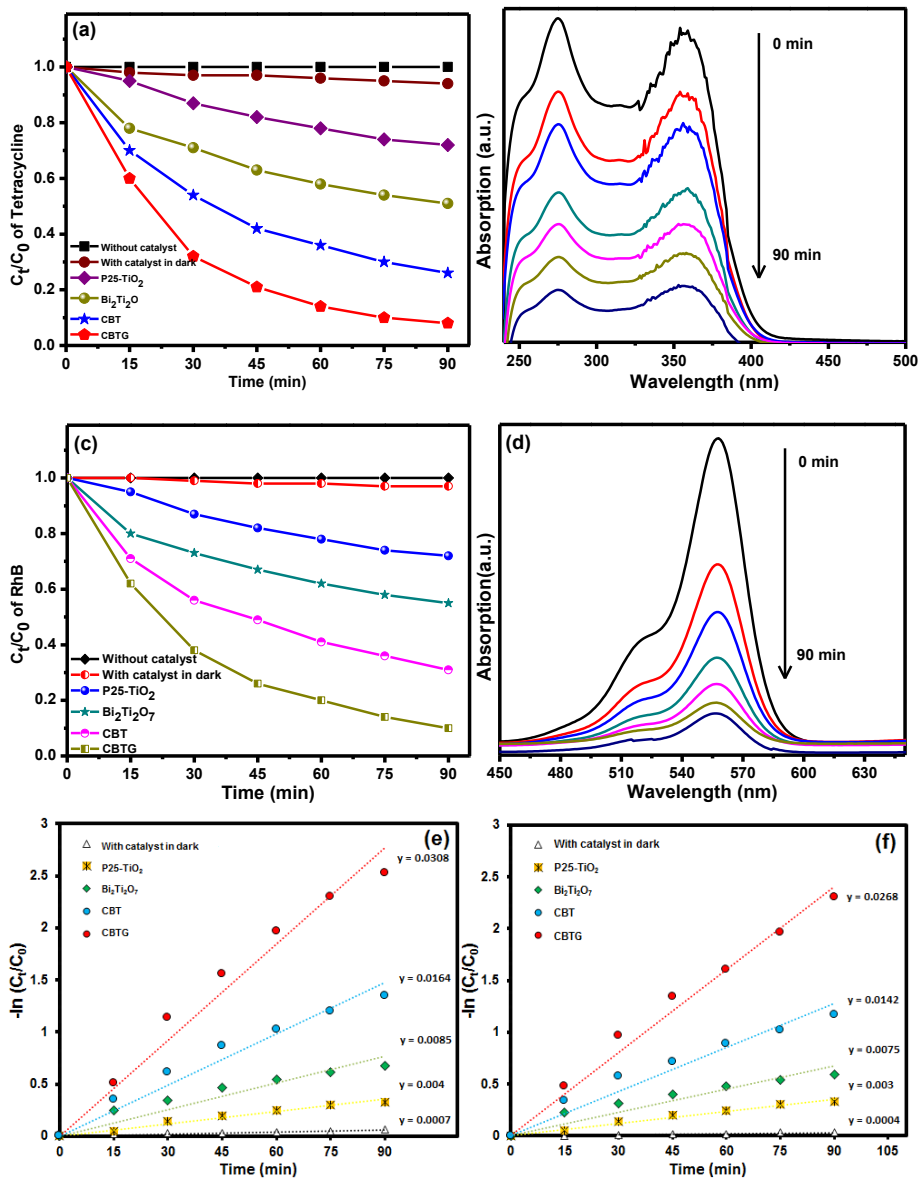


Fig. 11: Photocatalytic degradation rate curves: (a) Tetracycline and (c) RhB, and degradation spectral changes of carcinogens: (b) Tetracycline and (d) RhB with CBTG photocatalyst and The

pseudo first order kinetics plot: (e) Tetracycline and (f) RhB (reaction condition: catalyst dosage = 100 mg, carcinogen concentration = 50 mg/L, pH = 7 and reaction time = 90 min).

The photocatalytic carcinogen degradation potential of the as-synthesized materials were examined by using tetracycline and RhB as a target model carcinogen under visible light irradiation for 90 min. The temporal concentration of tetracycline and RhB molecules were found by UV-Vis analysis with difference in their peak intensities in regular periodic time intervals and the degradation rates of tetracycline and RhB was shown in **Fig. 11**. The figure shows that the photocatalytic degradation rate of both tetracycline and RhB was higher when using CBTG ternary nanocomposite than the pristine $\text{Bi}_2\text{Ti}_2\text{O}_7$ and binary nanostructure as photocatalyst. The self-stability of tetracycline and RhB molecules were tested by dissolving them in deionized water and the results revealed that the tetracycline and RhB molecules were highly stable in the aqueous solution, it is due to self photodegradation of tetracycline and RhB molecules are very slow. The photodegradation tetracycline was found to be 49%, 74% and 92% and in the case of RhB, the photodegradation rate was found to be 45%, 69% and 90% in presence of pristine $\text{Bi}_2\text{Ti}_2\text{O}_7$, CBT and CBTG, respectively. To analyze the self-degradation property of carcinogens, the photocatalytic degradation examination was performed in absence of a photocatalyst. The catalytic ability of CBTG was also analyzed in absence of visible light irradiation. In both tetracycline and RhB degradation, it is observed that the photocatalytic ability of CBTG is much higher than the pristine and binary nanocomposite. Additionally, to examine the practical assessment of CBTG, the comparative photocatalytic experiment with P25- TiO_2 was also carried out. The results showed that the photocatalytic activity of P25- TiO_2 is much lower than that of CBTG composite. From the obtained results it was found that the composition of rGO with CBT was able to enhance the photocatalytic performance and the due to the presence of oxygen containing groups like ketonic (C=O) groups with several zig-zag edges in rGO, it is catalytically active towards organic element degradation. More specifically, these zig-zag ketonic groups are highly active due to the presence of surplus amount of electrons and this behaviour results to the great ability towards co-ordination of redox reaction process^{13,37}. Consequently, the addition of rGO to the CBT enhances the synergetic effect in the photocatalytic activity and the reactive species generation. The enhancement in chemical reactions at active sites and relative mass transfer rates is analogous to some other photocatalytic systems like TiO_2 -rGO⁴⁵, MnFe_2O_4 -rGO⁵⁰, CoFe_2O_4 /rGO⁵¹, and Co_3O_4 -rGO³⁶. Furthermore, the photocatalytic degradation kinetics of tetracycline and RhB carcinogens

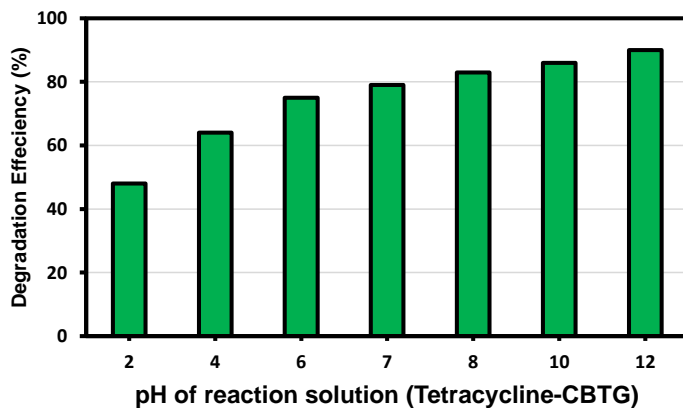
Commented [EG8]: Is there a general protocol for that from a previous study (ies)?

were studied in presence of as-synthesized photocatalysts and P25-TiO₂ photocatalyst. The results suggests that the degradation of tetracycline and RhB follows the pseudo first order kinetics as follow: $\ln\left(\frac{C_t}{C_0}\right) = k_{app} t$, where C_t and C_0 are temeporal concentration at time t and initial concentration of carcinogens respectively and k_{app} is the apparent first order photoreaction rate constant per minute¹². From Fig. 11e and 11f it can be extracted that CBTG shows enhanced photocatalytic degradation ability than CBT, P25-TiO₂ and Pristine Bi₂Ti₂O₇ nanostructures towards both tetracycline and RhB degradation. The photocatalytic degradation rate constant of CBTG is $k_{app} = 3.08 \times 10^{-2}$ and 2.68×10^{-2} for tetracycline and RhB degradation respectively. The degradation rate constant of CBTG is 7.7 times greater than P25-TiO₂ and 1.8 times greater than CBT towards tetracycline degradation and 8.9 times greater than P25-TiO₂ and 1.9 times greater than CBT towards RhB degradation. These obtained results suggests that photocatalytic degradation ability is highly improved when rGO and Cu is composited with Pristine Bi₂Ti₂O₇.

Commented [EG9]: Maybe to add a reference here?

3.9 Effect of operational parameters

3.9.1 Effect due to Initial pH of solution



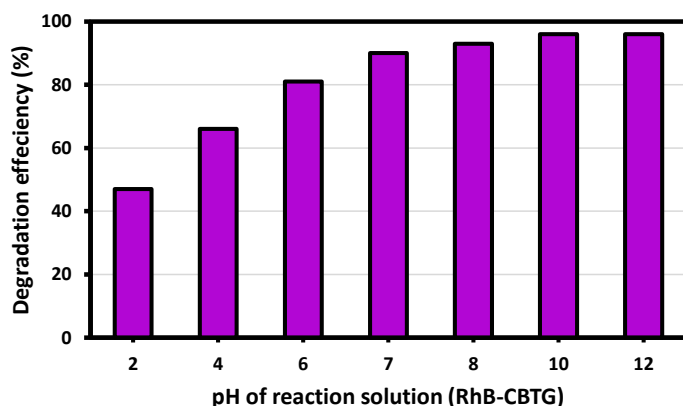


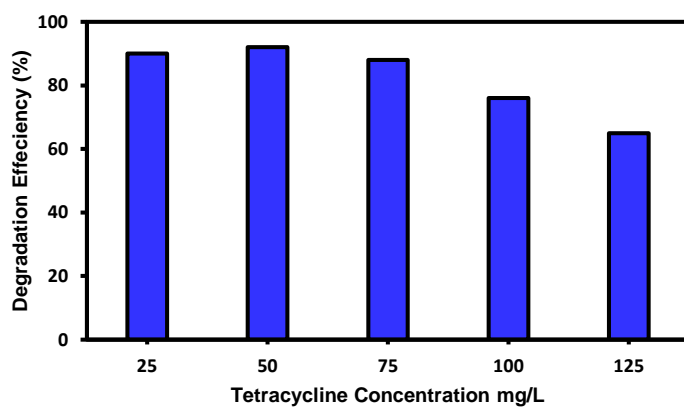
Fig. 12: Effect of pH value on degradation of (a) Tetracycline and (b) RhB (reaction condition: catalyst dosage = 100 mg, carcinogen concentration = 50 mg/L and reaction time = 45 min).

The organic carcinogenic molecules usually have a widespread range of pH value and hence pH of the reaction will play an important role in the characteristics of carcinogen molecules and also it influences on the surface charge properties of photocatalyst, the charge of carcinogen molecules, the size of catalytic aggregate formation, adsorption of carcinogenic molecules onto catalytic surface and the concentration of hydroxyl radicals ($\cdot\text{OH}$)³⁷. The photocatalytic efficiency of CBTG for degradation of tetracycline and RhB in different initial pH of the reaction solution varies from acidic to alkaline condition by using CBTG as photocatalytic material is presented in **Fig. 12**. From the obtained results it is found that the photodegradation of RhB and tetracycline molecules depends on the pH levels of the reaction solution. The results showed that an increase in the pH level of the reaction solution from 3 to 10, the photocatalytic degradation efficiency is also parallel for both tetracycline and RhB. The photocatalytic degradation of both tetracycline and RhB molecules were gradually decreasing when the pH of the reaction solution increased above 10. But the degradation rate of both the carcinogens is slightly similar at pH values of 7-10. From the obtained results it was found that the optimum pH for efficient photocatalytic degradation of tetracycline and RhB molecules by CBTG photocatalyst is 7. The photocatalytic degradation efficiency of the catalyst depends on the adsorption ability of the carcinogen

Commented [EG10]: Can you also refer to another study in the literature that mentioned similar results?

molecules. The adsorption of carcinogen molecules is influenced by the ionic nature of carcinogens and the surface ionic nature of photocatalyst. The tetracycline and RhB molecules are highly cationic nature and hence they will exist as positive ions at neutral pH and the surface charge of photocatalyst can be easily modified by changing the pH of reaction solution¹¹. The photocatalytic surface will become more anionic if the pH of reaction solution is increased above 7. The electrostatic force of attraction between negatively charged CBTG photocatalyst and positively charged carcinogen molecules may lead to sturdy adsorption of carcinogen molecules on the surface of CBTG photocatalyst. The higher adsorption of carcinogen molecules on the photocatalytic surface leads to the higher photocatalytic degradation.

3.9.2 Effect due to Initial concentration of dye



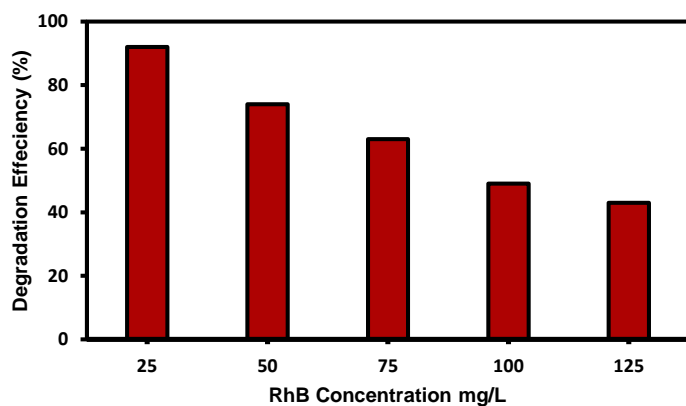


Fig. 13: Effect of carcinogen concentration on degradation of (a) Tetracycline and (b) RhB (reaction condition: catalyst dosage = 100 mg, pH = 7 and reaction time = 45 min).

The effect of the initial concentration upon the photocatalytic degradation of tetracycline and RhB by CBTG photocatalyst is illustrated in **Fig. 13**. The photocatalytic degradation of both tetracycline and RhB was examined in their various initial concentration (25, 50, 75, 100 and 125 mg/L) while all the rest parameters were maintained as explained in typical photodegradation reaction. The obtained results from **Fig. 13** shows that the photocatalytic degradation rates of both tetracycline and RhB were slowly decreased when increasing the carcinogen concentration. The decrement in photocatalytic degradation of carcinogen molecules at higher initial concentration is due to the insufficient amount of reactive species generation by the photocatalytic materials to degrade such higher amount of carcinogen molecules³⁷. The photon penetration ability through the reaction solution also plays a major role in the activation of photocatalyst to generate the reactive species results in the degradation of carcinogens⁵²⁻⁵⁵. But in higher initial concentration of carcinogens, the incident light gets screened by the carcinogen molecules and thus screening effect decreases the possibility of light to reach the photocatalyst and results to the shrinkage of photocatalytic performance.

3.10 Hydroxyl radical production analysis

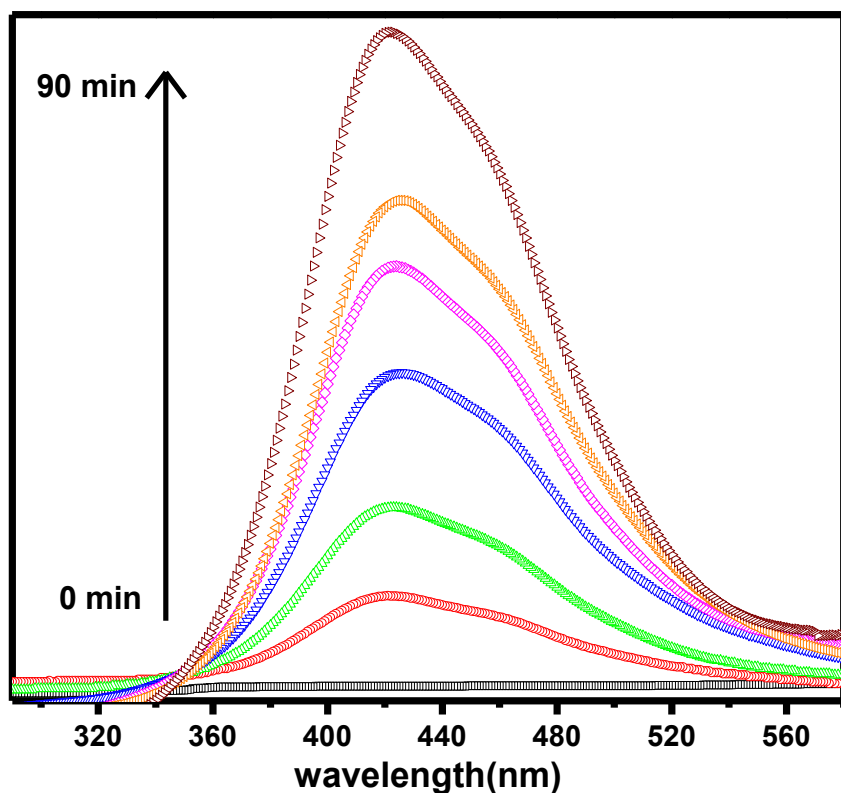


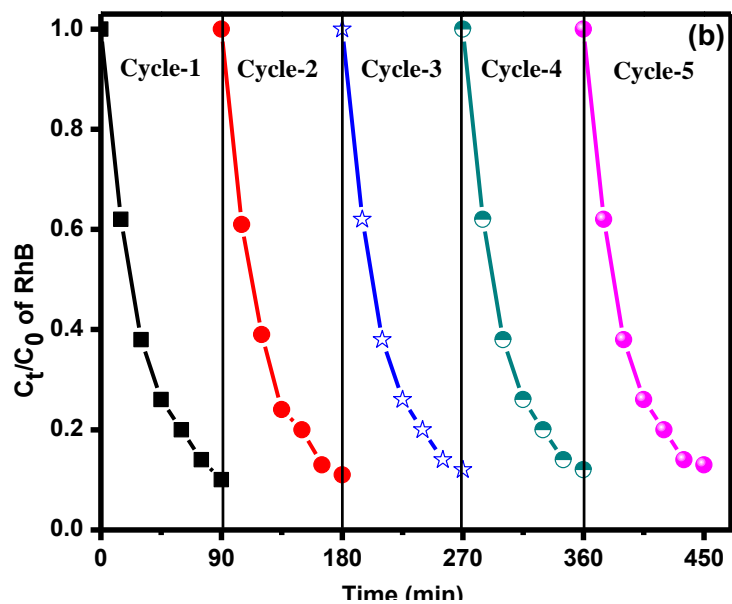
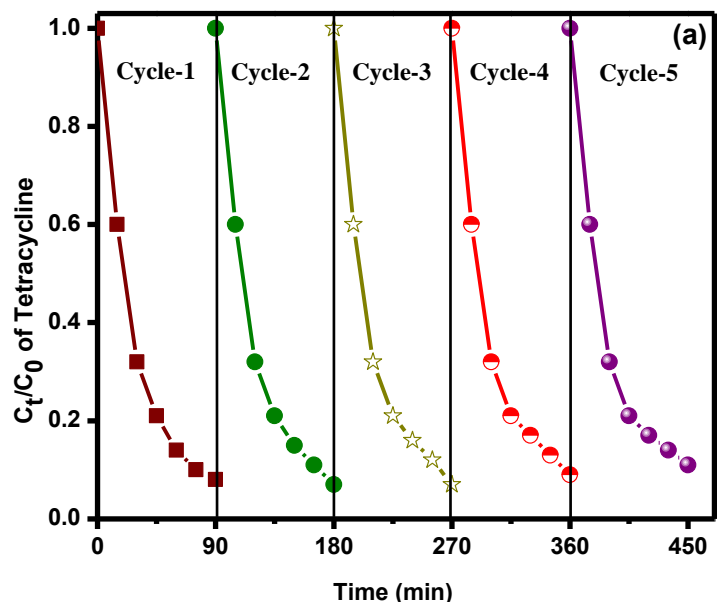
Fig. 14: PL spectrograph of 2-hydroxyterephthalic acid that formed upon the reaction between the $\cdot\text{OH}$ radicals produced by CBTG photocatalyst.

The production of $\cdot\text{OH}$ radicals from the as-synthesized CBTG photocatalyst under visible light irradiation was analyzed by terephthalic acid (TA) as a probe molecule as described in the experimental section. The absence of any absorbance peak in PL graphs represents no emissions from the TA solution. When CBTG photocatalyst was added to the TA solution, the broad peaks with emission at 425 nm represents the formation of 2-hydroxyterephthalic acid (HTA)²⁸. The HTA molecules are formed by the reaction of hydroxyl radicals with TA molecules which are generated

by the CBTG photocatalyst and it is confirmed by PL spectrographs as shown in **Fig. 14**. The increasing peak intensity with the visible light irradiation in presence of photocatalyst indicates the formation of a larger number of HTA molecules and it results from the increase in production rate of the $\cdot\text{OH}$ radicals in the solution. The obtained results showed that the CBTG photocatalyst can produce $\cdot\text{OH}$ radicals in a more efficient way. In the general pathway of the photocatalytic reaction, when the photocatalytic material is irradiated by photons with appropriate wavelength excites the electrons from the valance band (VB) to conduction band (CB) and leaving the equivalent holes in valence band (VB). When this electron charge separation is continued in photocatalytic material, the carcinogen molecules either oxidized or reduced through the acceptance or donation of electrons. The redox reaction is the key aspect of photocatalytic process and they are mainly determined by the band edge position of photocatalytic materials³⁵. In the case of CBTG photocatalyst, the electrons excited from VB to CB of $\text{Bi}_2\text{Ti}_2\text{O}_7$ are trapped by the Cu nanoparticles and the graphene sheets. Thus the trapping of electrons will restrict the recombination of e^- - h^+ pairs and in parallel the redox process will occur rapidly. The reaction of holes with OH^- ions leads to the generation of $\cdot\text{OH}$ radicals. When the electrons are trapped by Cu and rGO sheets, more amount of holes will react with OH^- ions to produce a higher amount of $\cdot\text{OH}$ radicals. In addition, these $\cdot\text{OH}$ radicals react with the carcinogen molecules and lead to the effective degradation of carcinogen molecules. In addition, the holes have a capability to react directly with carcinogen molecules and degrade the molecules¹¹. Hence, the observed net enhancement in photocatalytic degradation efficiency of CBTG photocatalyst is attributed to the effective charge carrier separation which is achieved by trapping excited electrons in photocatalyst⁵⁶. The delocalization of electrons in CB restricts their recombination with holes. So, these trapped electrons and separated holes were effectively reacted with surrounding medium and results to the effective photocatalytic degradation of carcinogen molecules.

Commented [EG11]: I believe that this sentence can be re-written on a more easy way to be understandable

3.11 Stability and recyclability Analysis



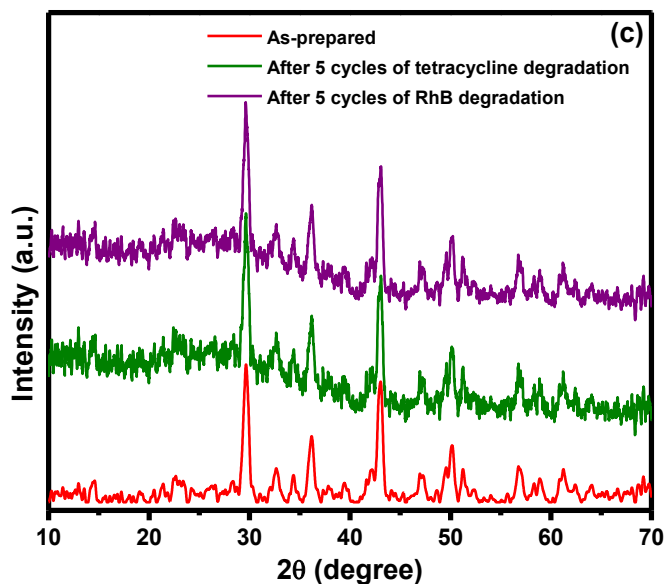


Fig. 15: Recyclable photodegradation performance of CBTG photocatalyst upon degrading (a) tetracycline and (b) RhB, and (c) XRD pattern of CBTG photocatalyst after 5th cycle of tetracycline and RhB degradation.

The catalytic stability is a significant parameter that describes the effectiveness of a photocatalytic material and can lead to a significant cost reduction of the carcinogen removal treatment if it is used for longer time slots. The reusability and stability of CBTC composite can be verified by performing a series of cycling experiments performed with optimal CBTG and the curves for 5 cycles of photocatalytic degradation of tetracycline and RhB are shown in **Fig. 15a and 15b**. This stability verification experiment was carried out for a protracted period of time (460 min) under typical photocatalytic reaction conditions. From the recycling experiments very small reduction in photocatalytic performance of CBTG was observed after 5 cycles of photocatalytic carcinogen degradation. This reduction of ~4% and ~3% in tetracycline and RhB degradation respectively after 5 cycles of photocatalytic degradation revealed that the as-synthesized CBTG composite can present high stability for practical photocatalytic applications. Furthermore, the XRD analysis of CBTG was also carried out after 5 cycles of tetracycline and RhB degradation

and the obtained spectrographs didn't show any phase change in CBTG photocatalyst (**Fig. 15c**). That reveals that the CBTG is stable even after 5 cycles of carcinogen degradation.

3.12 Photocatalytic mechanism

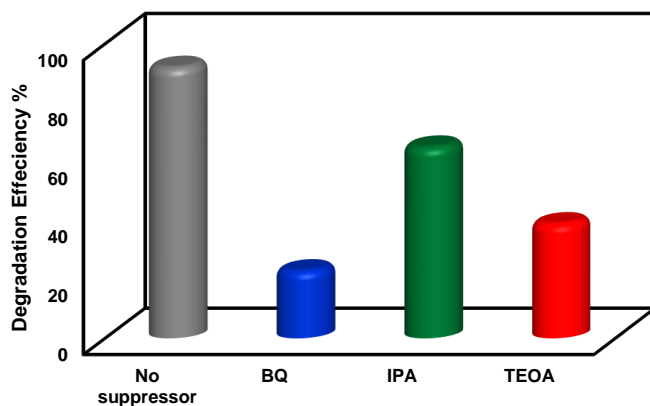
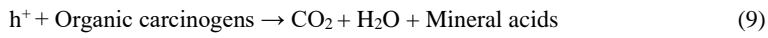
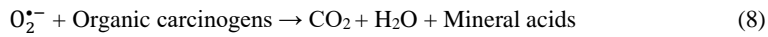
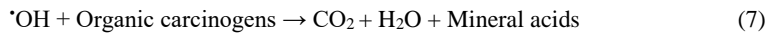
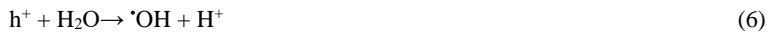
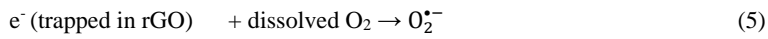
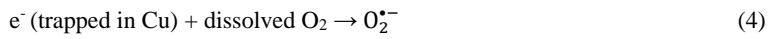
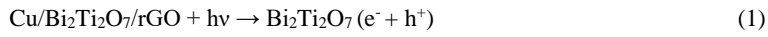


Fig. 16: Trapping experiment of active species during the photocatalytic degradation of tetracycline by CBTG (reaction condition: catalyst dosage = 100 mg, carcinogen concentration = 50 mg/L and reaction time = 90 min, pH=7).

During a photocatalytic process, redox reactions occur on the surface of the photocatalyst which successively produces reactive species such as $O_2^{\bullet-}$, $\cdot OH$ and h^+ , which are involved in the photodegradation process of organic molecules. The study on contribution of these oxidative species is important to elucidate the photocatalytic mechanism of CBTG photocatalyst. Hence, trapping experiments of the active species $O_2^{\bullet-}$, $\cdot OH$ and h^+ were carried out under visible light irradiation in presence of their respective trapping agents (as explained in section: 2.4). As shown in **Fig. 16**, the photocatalytic degradation efficiency of CBTG photocatalyst was effectively decreased and the degradation efficiency was found to be 23% while adding BQ ($O_2^{\bullet-}$ radical suppressor). When adding TEOA (h^+ suppressor) and IPA ($\cdot OH$ radical suppressor) the photocatalytic degradation efficiency of CBTG was affected up to 39% and 65% respectively. These results indicate that the $O_2^{\bullet-}$ radicals have the highest contribution than $\cdot OH$ and h^+ species during the photocatalytic degradation of organic molecules.

The possible photocatalytic mechanism of CBTG composite is proposed in **Fig. 17**, based on the previous experimental results. In general, the photo-excited electrons from valence band (VB) to conduction band (CB) are expended by the oxygen molecules adsorbed on the photocatalytic surface to generate superoxide radicals ($O_2^{\bullet-}$), at the same time holes generated in the valence band of photocatalytic material are scavenged by the hydroxyl groups to generate hydroxyl radicals ($\bullet OH$)^{10,57}. On the other hand, holes generated on the VB of photocatalyst can directly oxidize the organic carcinogen molecules. These generated radicals are utilized for degrading organic carcinogens. The photocatalytic degradation rate primarily depends on the concentration of photo-excited e^-h^+ pair remains without recombination¹⁹. In case of CBTG photocatalyst, the photoexcited electrons from VB of CBTG are trapped by the Cu nanoparticles and the rGO sheets which subsequently decreases the e^-h^+ pairs recombination and it results to the enhanced generation of reactive species like $O_2^{\bullet-}$ and $\bullet OH$ radicals. In order to understand the electron charge transfer between pristine $Bi_2Ti_2O_7$ and electron trappers, such as Cu nanoparticles and rGO sheets, the VB and CB band edge positions of pristine $Bi_2Ti_2O_7$ were calculated using following equations, $E_{CB} = \chi - E^C - 0.5 E_g$ and $E_{VB} = E_{CB} + E_g$ where χ is the electronegativity of the semiconductor, E^C is the energy of free electrons on the hydrogen scale of 4.5 eV, E_g is the band gap of semiconductor, E_{VB} and E_{CB} are valence band and conduction band energy¹¹. The electronegativity (χ) of $Bi_2Ti_2O_7$ can be expressed as an arithmetic mean of electron affinity between individual atoms (Bi-0.942362 eV, Ti-0.079 eV, O-1.4611134 eV) and their first ionization energy of atoms (Bi-7.2856 eV, Ti-6.8281 eV, O-13.6181 eV)⁵⁸. Based on the above values the VB and CB of $Bi_2Ti_2O_7$ is found to be 2.36 eV vs *NHE* and -0.52 eV vs *NHE*, respectively. When the Cu nanoparticles and rGO sheets are loaded with $Bi_2Ti_2O_7$ nanostructures the photo excited CB electrons of $Bi_2Ti_2O_7$ will transfer to these Cu nanoparticles and rGO sheets which causes e^-h^+ pair separation. The excited electrons of $Bi_2Ti_2O_7$ can be easily trapped by the Cu metal particles to prolong their lifetime due to their lower redox potential of Cu (+0.35 eV vs *NHE*) than the CB of $Bi_2Ti_2O_7$ (-0.52 eV vs *NHE*)⁵⁹. At the same time due to the lower fermi level of rGO (-0.08 eV vs *NHE*) than the CB of $Bi_2Ti_2O_7$ (-0.52 eV vs *NHE*), the CB electrons of $Bi_2Ti_2O_7$ will be successfully trapped by the rGO and it will decline the e^-h^+ pair recombination enormously by delocalizing photo-excited electrons on $Bi_2Ti_2O_7$. The enhanced trapping/delocalization of electrons by Cu nanoparticles and rGO sheets will effectively reduce the recombination rate of charge carriers and it will effectively lead to a higher generation of

reactive species for the degradation of carcinogens. Finally, the catalytic reaction of reactive species with organic carcinogens will mineralize the carcinogen molecules into CO₂, H₂O, and other organic ions. The possible photoexcited charge carrier delocalization and transportation pathway on CBTG photocatalyst will occur as the following equations (1) to (9)



The above discussed photocatalytic mechanism clearly shows that the both Cu nanoparticles and rGO sheets are acting as an excellent electron tappers to decrease recombination of e⁻- h⁺ pairs and it facilitates generation of large amount of O₂^{•-} radicals with successive degradation of organic molecules.

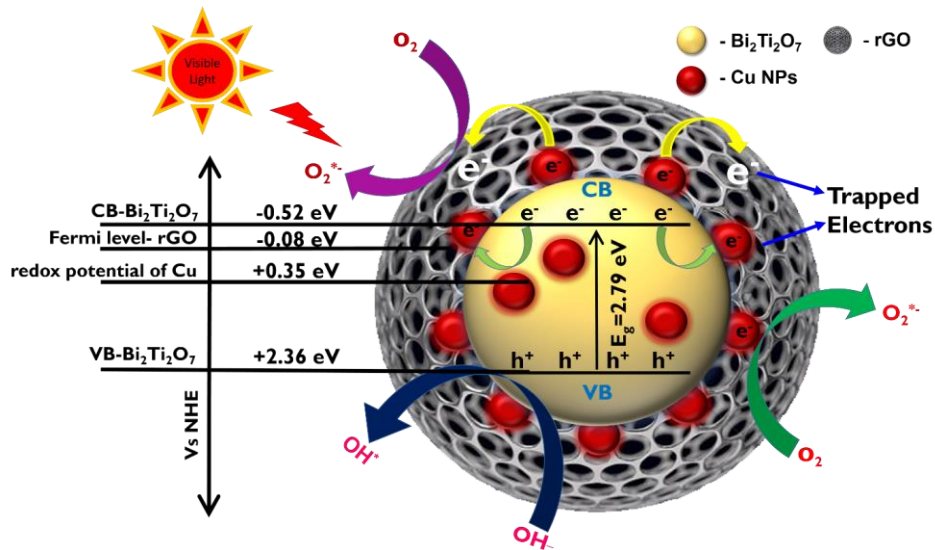


Fig. 17: Proposed photocatalytic mechanism of CBTG

4. Conclusion

In the current work, a novel Cu/ $Bi_2Ti_2O_7$ /rGO hybrid photocatalyst was successfully synthesized by following a simple hydrothermal method. The presence of both Cu nanoparticles and rGO sheets on $Bi_2Ti_2O_7$ was clearly observed by XRD analysis. The UV-Vis DRS analysis revealed that the Cu/ $Bi_2Ti_2O_7$ /rGO ternary nanocomposite is highly active within the visible region. The deposition of Cu nanoparticles on $Bi_2Ti_2O_7$ nanoparticles were analyzed and confirmed by HR-TEM analysis. The PL analysis revealed that the presence of Cu nanoparticles and rGO sheets on the $Bi_2Ti_2O_7$ photocatalyst is effectively decreasing the e^- - h^+ pair recombination. The photocatalytic degradation ability of as-synthesized pristine, binary and ternary nanocomposite was investigated in detail by using RhB and tetracycline as reference carcinogen molecules. The photocatalytic degradation results revealed that Cu/ $Bi_2Ti_2O_7$ /rGO photocatalyst is highly efficient than other as-prepared nanostructures. The photocatalytic degradation pathways of both RhB and tetracycline molecules were clearly illustrated and discussed. The analysis of the obtained results suggested that the Cu nanoparticles and the rGO sheets are playing major role in the photocatalytic ability of Cu/ $Bi_2Ti_2O_7$ /rGO photocatalyst. From

trapping experiments, it was found that $O_2^{\bullet-}$ radicals can be massively generated by Cu/Bi₂Ti₂O₇/rGO photocatalyst. The passage of the photoexcited electrons and its trapping on Cu nanoparticles and rGO sheets were clearly explained in the photocatalytic mechanism. In addition, the Cu/Bi₂Ti₂O₇/rGO photocatalyst showed higher stability and recyclability even after five cycles of carcinogen degradation. The strategy of using CB electron trappers on photocatalytic materials are expected to inspire future development of high efficient photocatalytic materials for organic carcinogen molecule degradation.

Commented [EG12]: Not quite sure if this necessary

Reference

- (1) Sandin, G.; Peters, G. M. Environmental Impact of Textile Reuse and Recycling – A Review. *J. Clean. Prod.* **2018**, *184*, 353–365.
- (2) Biran Ay, S.; Kosku Perkgoz, N. Reduced Graphene Oxide and Ag Wrapped TiO₂ Photocatalyst for Enhanced Visible Light Photocatalysis. *J. Nanomater.* **2015**, *2015*.
- (3) Yang, Z.-M.; Huang, G.-F.; Huang, W.-Q.; Wei, J.-M.; Yan, X.-G.; Liu, Y.-Y.; Jiao, C.; Wan, Z.; Pan, A. Novel Ag₃PO₄/CeO₂ Composite with High Efficiency and Stability for Photocatalytic Applications. *J. Mater. Chem. A* **2014**, *2* (6), 1750–1756.
- (4) Jinhai, L.; Han, M.; Guo, Y.; Wang, F.; Meng, L.; Mao, D.; Ding, S.; Sun, C. Hydrothermal Synthesis of Novel Flower-like BiVO₄/Bi₂Ti₂O₇ with Superior Photocatalytic Activity toward Tetracycline Removal. *Appl. Catal. A Gen.* **2016**, *524*, 105–114.
- (5) Chen, F.; Yang, Q.; Sun, J.; Yao, F.; Wang, S.; Wang, Y.; Wang, X.; Li, X.; Niu, C.; Wang, D.; et al. Enhanced Photocatalytic Degradation of Tetracycline by AgI/BiVO₄ Heterojunction under Visible-Light Irradiation: Mineralization Efficiency and Mechanism. *ACS Appl. Mater. Interfaces* **2016**, *8* (48), 32887–32900.
- (6) Reyes, C.; Fernández, J.; Freer, J.; Mondaca, M. A.; Zaror, C.; Malato, S.; Mansilla, H. D. Degradation and Inactivation of Tetracycline by TiO₂ photocatalysis. *J. Photochem. Photobiol. A Chem.* **2006**, *184* (1–2), 141–146.
- (7) Aretxaga, A.; Romero, S.; Sarrà, M.; Vicent, T. Adsorption Step in the Biological Degradation of a Textile Dye. *Biotechnol. Prog.* **2001**, *17* (4), 664–668.

- (8) Zhu, T.; Chen, J. S.; Lou, X. W. Highly Efficient Removal of Organic Dyes from Waste Water Using Hierarchical NiO Spheres with High Surface Area. *J. Phys. Chem. C* **2012**, *116* (12), 6873–6878.
- (9) Ng, S. W. L.; Yilmaz, G.; Ong, W. L.; Ho, G. W. One-Step Activation towards Spontaneous Etching of Hollow and Hierarchical Porous Carbon Nanospheres for Enhanced Pollutant Adsorption and Energy Storage. *Appl. Catal. B Environ.* **2018**, *220*, 533–541.
- (10) Wang, W.; Wang, Z.; Liu, J.; Luo, Z.; Suib, S. L.; He, P.; Ding, G.; Zhang, Z.; Sun, L. Improved Visible Light Photocatalytic Activity of RGO-Fe₃O₄-NiO Hybrid Nanocomposites Synthesized by in-Situ Facile Method for Industrial Wastewater Treatment Applications. *Sci. Rep.* **2017**, *7* (March), 46610.
- (11) Shanavas, S.; Priyadharsan, A.; Vasanthakumar, V.; Arunkumar, A.; Anbarasan, P. M.; Bharathkumar, S. Mechanistic Investigation of Visible Light Driven Novel La₂CuO₄/CeO₂/RGO Ternary Hybrid Nanocomposites for Enhanced Photocatalytic Performance and Antibacterial Activity. *J. Photochem. Photobiol. A Chem.* **2017**, *340*, 96–108.
- (12) Shajahan, S.; Arumugam, P.; Rajendran, R.; Ponnusamy Munusamy, A. Optimization and Detailed Stability Study on Pb Doped Ceria Nanocubes for Enhanced Photodegradation of Several Anionic and Cationic Organic Pollutants. *Arab. J. Chem.* **2017**.
- (13) Wei, Q.; Wang, Y.; Qin, H.; Wu, J.; Lu, Y.; Chi, H.; Yang, F.; Zhou, B.; Yu, H.; Liu, J. Construction of RGO Wrapping Octahedral Ag-Cu₂O Heterostructure for Enhanced Visible Light Photocatalytic Activity. *Appl. Catal. B Environ.* **2018**, *227*, 132–144.
- (14) Subash, B.; Krishnakumar, B.; Swaminathan, M.; Shanthi, M. Highly Efficient, Solar Active, and Reusable Photocatalyst: Zr-Loaded Ag-ZnO for Reactive Red 120 Dye Degradation with Synergistic Effect and Dye-Sensitized Mechanism. *Langmuir* **2013**, *29* (3), 939–949.
- (15) Gupta, S.; Subramanian, V. Encapsulating Bi₂Ti₂O₇(BTO) with Reduced Graphene Oxide (RGO): An Effective Strategy to Enhance Photocatalytic and Photoelectrocatalytic

Activity of BTO. *ACS Appl. Mater. Interfaces* **2014**, *6* (21), 18597–18608.

- (16) Xia, B. Y.; Wu, H. Bin; Chen, J. S.; Wang, Z.; Wang, X.; Lou, X. W. (David). Formation of Pt–TiO₂–rGO 3-Phase Junctions with Significantly Enhanced Electro-Activity for Methanol Oxidation. *Phys. Chem. Chem. Phys.* **2012**, *14* (2), 473–476.
- (17) Zhang, N.; Zhang, Y.; Pan, X.; Yang, M. Q.; Xu, Y. J. Constructing Ternary CdS-Graphene-TiO₂ Hybrids on the Flatland of Graphene Oxide with Enhanced Visible-Light Photoactivity for Selective Transformation. *J. Phys. Chem. C* **2012**, *116* (34), 18023–18031.
- (18) Tang, Z.-R.; Zhang, Y.; Zhang, N.; Xu, Y.-J. New Insight into the Enhanced Visible Light Photocatalytic Activity over Boron-Doped Reduced Graphene Oxide. *Nanoscale* **2015**, *7* (16), 7030–7034.
- (19) Liu, T.; Liu, B.; Yang, L.; Ma, X.; Li, H.; Yin, S.; Sato, T.; Sekino, T.; Wang, Y. RGO/Ag₂S/TiO₂ ternary Heterojunctions with Highly Enhanced UV-NIR Photocatalytic Activity and Stability. *Appl. Catal. B Environ.* **2017**, *204*, 593–601.
- (20) Qian, K.; Xia, L.; Wei, W.; Chen, L.; Jiang, Z.; Jing, J.; Xie, J. Construction of Bi₂Ti₂O₇/Bi₄Ti₃O₁₂ composites with Enhanced Visible Light Photocatalytic Activity. *Mater. Lett.* **2017**, *206* (3), 245–248.
- (21) Du, Y.; Hao, Q.; Chen, D.; Chen, T.; Hao, S.; Yang, J.; Ding, H.; Yao, W.; Song, J. Facile Fabrication of Heterostructured Bismuth Titanate Nanocomposites: The Effects of Composition and Band Gap Structure on the Photocatalytic Activity Performance. *Catal. Today* **2017**, *297*, 255–263.
- (22) Zhang, Z.; Jiang, C.; Du, P.; Wang, Y. Synthesis and Characterization of Bi₂Ti₂O₇/TiO₂ heterojunction by Glycerol-Assisted Alcoholthermal Method. *Ceram. Int.* **2015**, *41* (3), 3932–3939.
- (23) Zhou, D.; Yang, H.; Tu, Y.; Tian, Y.; Cai, Y.; Hu, Z.; Zhu, X. In Situ Fabrication of Bi₂Ti₂O₇/TiO₂ Heterostructure Submicron Fibers for Enhanced Photocatalytic Activity. *Nanoscale Res. Lett.* **2016**, *11* (1), 193.
- (24) Gawande, M. B.; Goswami, A.; Felpin, F. X.; Asefa, T.; Huang, X.; Silva, R.; Zou, X.;

Zboril, R.; Varma, R. S. Cu and Cu-Based Nanoparticles: Synthesis and Applications in Catalysis. *Chem. Rev.* **2016**, *116* (6), 3722–3811.

- (25) Wu, X.; Xing, Y.; Pierce, D. T.; Zhao, J. X. One-Pot Synthesis of Reduced Graphene Oxide/Metal (Oxide) Composites. *ACS Appl. Mater. Interfaces* **2017**, acsami.7b12539.
- (26) Hummers, W. S.; Offeman, R. E. Preparation of Graphitic Oxide. *J. Am. Chem. Soc.* **1958**, *80* (6), 1339.
- (27) Shahriary, L.; Athawale, A. a. Graphene Oxide Synthesized by Using Modified Hummers Approach. *Int. J. Renew. Energy Environ. Eng.* **2014**, *02* (01), 58–63.
- (28) Xiang, Q.; Yu, J.; Wong, P. K. Quantitative Characterization of Hydroxyl Radicals Produced by Various Photocatalysts. *J. Colloid Interface Sci.* **2011**, *357* (1), 163–167.
- (29) Prabhu, Y. T.; Venkateswara Rao, K.; Sessa Sai, V.; Pavani, T. A Facile Biosynthesis of Copper Nanoparticles: A Micro-Structural and Antibacterial Activity Investigation. *J. Saudi Chem. Soc.* **2017**, *21* (2), 180–185.
- (30) Khan, A.; Rashid, A.; Younas, R.; Chong, R. A Chemical Reduction Approach to the Synthesis of Copper Nanoparticles. *Int. Nano Lett.* **2016**, *6* (1), 21–26.
- (31) Primo, A.; Esteve-Adell, I.; Blandez, J. F.; Dhakshinamoorthy, A.; Álvaro, M.; Candu, N.; Coman, S. M.; Parvulescu, V. I.; Garóia, H. High Catalytic Activity of Oriented 2.0.0 Copper(I) Oxide Grown on Graphene Film. *Nat. Commun.* **2015**, *6* (4).
- (32) Jiang, H. G.; Rühle, M.; Lavernia, E. J. On the Applicability of the X-Ray Diffraction Line Profile Analysis in Extracting Grain Size and Microstrain in Nanocrystalline Materials. *J. Mater. Res.* **1999**, *14* (2), 549–559.
- (33) Koutsopoulos, S.; Barfod, R.; Eriksen, K. M.; Fehrmann, R. Synthesis and Characterization of Iron-Cobalt (FeCo) Alloy Nanoparticles Supported on Carbon. *J. Alloys Compd.* **2017**, *725*, 1210–1216.
- (34) Hou, J.; Cao, R.; Wang, Z.; Jiao, S.; Zhu, H. Chromium-Doped Bismuth Titanate Nanosheets as Enhanced Visible-Light Photocatalysts with a High Percentage of Reactive {110} Facets. *J. Mater. Chem.* **2011**, *21* (20), 7296.

- (35) Ji, Z.; Shen, X.; Yang, J.; Zhu, G.; Chen, K. A Novel Reduced Graphene Oxide/Ag/CeO₂ternary Nanocomposite: Green Synthesis and Catalytic Properties. *Appl. Catal. B Environ.* **2014**, *144*, 454–461.
- (36) Feng, Q.; Li, X.; Wang, J.; Gaskov, A. M. Reduced Graphene Oxide (RGO) Encapsulated Co₃O₄ Composite Nanofibers for Highly Selective Ammonia Sensors. *Sensors Actuators, B Chem.* **2016**, *222*, 864–870.
- (37) Yao, Y.; Xu, C.; Yu, S.; Zhang, D.; Wang, S. Facile Synthesis of Mn₃O₄-Reduced Graphene Oxide Hybrids for Catalytic Decomposition of Aqueous Organics. *Ind. Eng. Chem. Res.* **2013**, *52* (10), 130226103026006.
- (38) Mahboob, S.; Prasad, G.; Chou, C. C.; Kumar, G. S. Electrical and X-Ray Photoelectron Spectroscopy Study on (Na_{0.5}-XK XBi_{0.5}-XNd_x)TiO₃ Ceramics. *Ferroelectrics* **2013**, *445* (1), 161–171.
- (39) Hou, J.; Jiao, S.; Zhu, H.; Kumar, R. V. Carbon-Modified Bismuth Titanate Nanorods with Enhanced Visible-Light-Driven Photocatalytic Property. *CrystEngComm* **2011**, *13* (14), 4735.
- (40) Yi, J.; Yuan, X.; Wang, H.; Yu, H.; Peng, F. Preparation of Bi₂Ti₂O₇/TiO₂ Nanocomposites and Their Photocatalytic Performance under Visible Light Irradiation. *Mater. Des.* **2015**, *86*, 152–155.
- (41) Li, L.; Yan, J.; Wang, T.; Zhao, Z.-J.; Zhang, J.; Gong, J.; Guan, N. Sub-10 Nm Rutile Titanium Dioxide Nanoparticles for Efficient Visible-Light-Driven Photocatalytic Hydrogen Production. *Nat. Commun.* **2015**, *6* (May 2014), 5881.
- (42) Wang, Y.; Tang, Y.; Chen, Y.; Li, Y.; Liu, X.; Luo, S.; Liu, C. Reduced Graphene Oxide-Based Photocatalysts Containing Ag Nanoparticles on a TiO₂ Nanotube Array. *J. Mater. Sci.* **2013**, *48* (18), 6203–6211.
- (43) Santoni, A.; Biccari, F.; Malerba, C.; Valentini, M.; Chierchia, R.; Mittiga, A. Valence Band Offset at the CdS/Cu₂ZnSnS₄ Interface Probed by x-Ray Photoelectron Spectroscopy. *J. Phys. D. Appl. Phys.* **2013**, *46* (17).

- (44) Ji, R.; Sun, W.; Chu, Y. One-Step Hydrothermal Synthesis of Ag/Cu₂O Heterogeneous Nanostructures over Cu Foil and Their SERS Applications. *RSC Adv.* **2014**, *4* (12), 6055.
- (45) El-Bery, H. M.; Matsushita, Y.; Abdel-moneim, A. Fabrication of Efficient TiO₂-RGO Heterojunction Composites for Hydrogen Generation via Water-Splitting: Comparison between RGO, Au and Pt Reduction Sites. *Appl. Surf. Sci.* **2017**, *423*, 185–196.
- (46) Liu, P.; Wang, H.; Li, X.; Rui, M.; Zeng, H. Localized Surface Plasmon Resonance of Cu Nanoparticles by Laser Ablation in Liquid Media. *RSC Adv.* **2015**, *5* (97), 79738–79745.
- (47) Xiong, L.; Xiao, H.; Zeng, Q.; Wang, B.; Wen, S.; Li, B.; Ding, Y.; Yu, H. Direct Transformation of Metallic Copper to Copper Nanostructures by Simple Alcohol Thermal Treatment and Their Photoactivity. *RSC Adv.* **2015**, *5* (119), 98344–98349.
- (48) Krasnov, A. G.; Piir, I. V.; Koroleva, M. S.; Sekushin, N. A.; Ryabkov, Y. I.; Piskaykina, M. M.; Sadykov, V. A.; Sadovskaya, E. M.; Pelipenko, V. V.; Eremeev, N. F. The Conductivity and Ionic Transport of Doped Bismuth Titanate Pyrochlore Bi_{1.6}M_xTi₂O₇ – δ(M – Mg, Sc, Cu). *Solid State Ionics* **2017**, *302*, 118–125.
- (49) Riaz, N.; Chong, F. K.; Man, Z. B.; Khan, M. S.; Dutta, B. K. Photodegradation of Orange II under Visible Light Using Cu-Ni/TiO₂: Influence of Cu: Ni Mass Composition, Preparation, and Calcination Temperature. *Ind. Eng. Chem. Res.* **2013**, *52* (12), 4491–4503.
- (50) Fu, Y. S.; Xiong, P.; Chen, H. Q.; Sun, X. Q.; Wang, X. High Photocatalytic Activity of Magnetically Separable Manganese Ferrite-Graphene Heteroarchitectures. *Ind. Eng. Chem. Res.* **2012**, *51* (2), 725–731.
- (51) Yao, Y.; Yang, Z.; Zhang, D.; Peng, W.; Sun, H.; Wang, S. Magnetic CoFe₂O₄ – Graphene Hybrids: Facile Synthesis, Characterization, and Catalytic Properties. *Ind. Eng. Chem. Res.* **2012**, *51* (17), 6044–6051.
- (52) Jamil, T. S.; Ghaly, M. Y.; Fathy, N. A.; Abd El-Halim, T. A.; Österlund, L. Enhancement of TiO₂ behavior on Photocatalytic Oxidation of MO Dye Using TiO₂/AC under Visible Irradiation and Sunlight Radiation. *Sep. Purif. Technol.* **2012**, *98*, 270–279.
- (53) Yu, K.; Yang, S.; He, H.; Sun, C.; Gu, C.; Ju, Y. Visible Light-Driven Photocatalytic

Degradation of Rhodamine B over NaBiO₃: Pathways and Mechanism. *J. Phys. Chem. A* **2009**, *113* (37), 10024–10032.

- (54) He, Z.; Sun, C.; Yang, S.; Ding, Y.; He, H.; Wang, Z. Photocatalytic Degradation of Rhodamine B by Bi₂WO₆ with Electron Accepting Agent under Microwave Irradiation: Mechanism and Pathway. *J. Hazard. Mater.* **2009**, *162* (2–3), 1477–1486.
- (55) Natarajan, T. S.; Thomas, M.; Natarajan, K.; Bajaj, H. C.; Tayade, R. J. Study on UV-LED/TiO₂ process for Degradation of Rhodamine B Dye. *Chem. Eng. J.* **2011**, *169* (1–3), 126–134.
- (56) Xu, Y.; Huang, S.; Xie, M.; Li, Y.; Jing, L.; Xu, H.; Zhang, Q.; Li, H. Core-shell Magnetic Ag/AgCl@Fe₂O₃ Photocatalysts with Enhanced Photoactivity for Eliminating Bisphenol A and Microbial Contamination. *New J. Chem.* **2016**, *40* (4), 3413–3422.
- (57) Liu, M.; Xue, X.; Yu, S.; Wang, X.; Hu, X.; Tian, H.; Chen, H.; Zheng, W. Improving Photocatalytic Performance from Bi₂WO₆@MoS₂/Graphene Hybrids via Gradual Charge Transferred Pathway. *Sci. Rep.* **2017**, *7* (1), 1–11.
- (58) Benčina, M.; Valant, M. Bi₂Ti₂O₇-Based Pyrochlore Nanoparticles and Their Superior Photocatalytic Activity under Visible Light. *J. Am. Ceram. Soc.* **2018**, *101* (1), 82–90.
- (59) Tahir, M.; Tahir, B. Dynamic Photocatalytic Reduction of CO₂ to CO in a Honeycomb Monolith Reactor Loaded with Cu and N Doped TiO₂ nanocatalysts. *Appl. Surf. Sci.* **2016**, *377*, 244–252.